NTNU – Trondheim
Norwegian University of
Science and Technology

Freeze-bond strength experiments,

radially confined compression tests on saline
and fresh water samples.

Ida Mari Bueide

Preface

This thesis is delivered upon the end of my master's degree in Civil and Environmental Engineering at the Norwegian University of Science and Technology. With the specialization topic of Marin Civil Engineering.

Freeze-bond strength experiments, specifically radially confined compression tests on saline and fresh water samples, were conducted at The University Center in Svalbard, spring 2014. This work could not have been done without good help from several individuals.

The idea to this project was a combination of guidance from my supervisor, Professor Knut Vilhelm Høyland, and an inspiring stay at UNIS fall 2013.

Svalbard, Longyearbyen, 2014-6-15

( )

Ida Mari Bueide

Acknowledgment

Firstly I would like to give thanks to my supervisor Knut Vilhelm Høyland who gave me the opportunity to conduct this thesis and encouraged my stay at UNIS. He has been a great support during my work. As well Jan Otto Larsen, my co-supervisor and professor at UNIS.

Alexey Shestov have been an invaluable person during my lab-work, both concerning the practical work and for discussion. Together with Kåre Johansen at logistics, who always has a ready hand to whatever predicament, they have eased my work greatly.

I would also like to thank all my good friends from the university and Kristoffer Hjellen for always believing in me and being an encouragement through all my time as a student. Finally I am grateful for Mikkel Arne Kristiansen, who has not only been a great help during my long hours of lab-work, but has been a source of support and made this spring memorable.

Ida Mari Bueide

Abstract

This thesis presents and analyses the method and results from strength experiments on freeze-bonds conducted on radially confined cylindrical samples (tri-axial tests). In total sixty samples were tested successfully, divided on twenty configurations. The variables consisted of confinement, submersion time, initial temperature and salinity (8 configurations with fresh water ice and 12 with 2-3ppt saline ice). The test set-up was similar to that of Møllegaard [2012] and Shafrova and Høyland [2008], uni-axial experiments were also conducted in order to ensure comparability. The measured freeze-bond shear stress found for the uni-axial samples were in the range of 170 - 800kPa (submersion times of 0.5 - 20 min).

The objective was to study the internal freeze-bond stress in relation to increasing radial confinement together with the variables; salinity, initial temperature and submersion time. And as well how to best conduct these experiments.

A large part of the configurations gave increasing stress for increasing confinement, both when studying the peak and residual stress plots. Mohr-Coulomb failure criterion was applied, the peak stress plots gave estimated cohesion values in the range 0.003 - 0.099 MPa and $16.21 - 44.70°$ for internal friction. For the residual stresses the cohesion values were approaching zero and the internal frictions were in the range $11.21 - 36.70°$. In relation to initial temperature the lowest initial temperature of -8.5°C gave the highest cohesion values. And the configurations with fresh samples were found to have a mean cohesion value 30% higher than for the saline.

Keywords: freeze-bond strength, radial confinement, triaxial.

Samandrag

Denne oppgåva presenterer og analyserer metodar og resultat frå styrke forsøk på fryseband utført på sylinderprøver med radielt trykk. Totalt sekti prøver vart testa fordelt på tjue konfigurasjonar. Variablane bestod av radielt trykk, neddykkingstid, start temperatur og salinitet (8 konfigurasjonar med fersk vatn og 12 med 2-3ppt saltvatnsis). Same test set-up som for Møllegaard [2012] og Shafrova and Høyland [2008] vart brukt og enaksielle testar vart utført for at resultata skulle vere samanliknbare. Fryseband styrken for dei enaksielle prøvene vart målt til 170 - 800kPa for neddykkingstidene 0.5 - 20 min.

Målet med denne oppgåva var å studere fryseband styrken i forhold til aukande radielt trykk, også i forhold til salinitet, start temperatur og neddykkingstid. Eit anna viktig formål var å arbeide gjennom korleis slike forsøk best kan utførast.

Ein stor del av konfigurasjonane gav aukande styrke for aukande radielt trykk, både for maks stress og residual stress. Mohr-Coulomb kriterie vart brukt og kohesjonsverdiar for maksimal stress vart funne til å ligge mellom 0.003 - 0.099 MPa og friksjonsverdiar frå 16.21 til $44.70°$. For residual stress var kohesjonsverdiane tilnærma null og friksjonsverdiane låg mellom $11-21 - 36.70°$. Start temperaturen på -8.5°C gav dei høgaste kohesjonsverdiane og konfigurasjonane med ferskvatns prøver hadde 30% høgare kohesjonsverdiar enn for saltvatns konfigurasjonane.

Keywords: fryseband, radiellt trykk, treaksiell.

Contents

Chapter 1

Introduction

1.1 Background

A common feature seen in the Arctic is sea ice ridges. First-year ice ridges and icebergs are considered to be the governing design load of offshore structures and ice breaking vessels. As oil- and gas-exploration enters these areas, further knowledge of the failure processes of ridges are needed. Ice ridges can also scour the sea floor in shallow water, which implicates in the design of sub-sea structures and pipelines.

The calculation of forces from ice ridges involves both the consolidated layer and the ice rubble. The ice rubble strength derives from the freeze-bonding and interlocking of ice blocks.

Repetto-Llamazares et al. [2011a], Repetto-Llamazares et al. [2011b] Repetto-Llamazares and Serré [2011] have recently published articles concerning freeze-bond strength. The two first on single freeze-bonds and the last on freeze-bonds as a part of the failure process in shear-box tests. Three projects on the topic of single freeze-bonds have been delivered at NTNU. Astrup [2012] investigating freeze-bond mechanism in rubble, Helgøy [2012] investigating freeze-bonds strength between two saline ice blocks in relation to physical properties and Møllegaard [2012] studying how the freeze-bond varies in the plane and also the freeze-bond strength in relation to several physical properties.

Developing a material model of an ice ridge is a long term process and determining how the freeze-bond depends on physical properties is a part of this process.

1.2 Research question and method

In this thesis the objective is to study the internal freeze-bond stresses in relation to an increase in radial confinement. The freeze-bond strength dependency on confinement have earlier been investigated by applying loads on top of ice blocks frozen together. A linear increase with increasing

confinement has been suggested and that a Mohr-Coulomb failure criterion may be suitable to describe the material.

The experiments in this thesis were conducted to investigate this further and to give estimated values of cohesion and internal friction to describe the material strength. As well as to study the failure mode and if it could be discerned from the plotted force.

The process of how to conduct compression tests on cylindrical samples with radial confinement was also an important part of this thesis.

Chapter 2

Theory

2.1 First-year ice ridges and freeze-bonds

Ice ridges are formed by compression and shearing in the ice cover, causing build-up of broken ice pieces, often in the length of the interaction zones between level ice floes. They can rise several meters above sea level and tens of meters below. The structure of an ice ridge is usually divided into the sail and keel. The sail is defined as the part above sea level and consists of ice blocks, in some cases snow, and voids filled with air and/or snow. The keel makes up the part under sea level and can again be divided into two layers; the consolidated layer and ice rubble. The consolidated layer found just below the sea line consists of ice rubble frozen together by water-filled voids that have frozen over. The rubble layer consists of ice blocks with water filled voids, the macro porosity of this layer is normally in the order of 20-40%. Touching ice blocks may form freeze-bonds in the initial stage of consolidation. The ratio between the keel hight and sail hight is found to be in the range of 4-5 [Timco and Burden, 1997]. An idealized ridge is illustrated in figure 2.1.
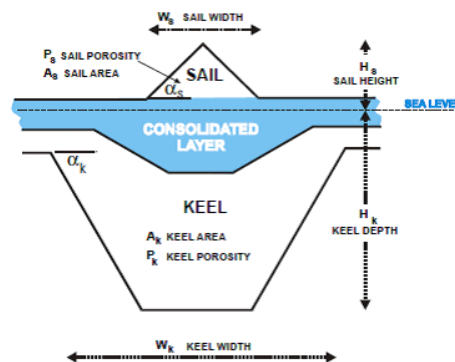

Figure 2.1: Illustration of an idealized ice-ridge from Timco and Burden [1997]

The strength of an ice ridge is dependent on the mechanical properties and the structure of the

ice ridge, which also means that the strength will change during its lifetime. To know how the strength of an ice ridge changes during its lifetime and to define parameter values, the failure mode and what parameters influences the strength needs to be defined. The total strength of a first-year ice ridge is believed to be a sum of the strength of the consolidated layer and the ice rubble. The last part may be divided into the keel-rubble and the sail, which has been found to have different mechanical properties.

$$F = Fc + Fk + (Fs) \tag{2.1}$$

Ettema and Urroz [1989] discuss the complex shear behaviour of unconsolidated ice rubble, it is argued that freeze-bonds govern the initial strength. Liferov and Bonnemaire [2005] concluded that the primary failure mode is controlled by the initial strength of the rubble skeleton, i.e. by freeze bonds between blocks inside the rubble. There is now an agreement that the failure of the freeze-bonds is the mechanism causing the peak load during the initial interaction between ice rubble and structure. Shafrova and Høyland [2008] suggested three failure mechanisms of the unconsolidated rubble

- Strength of freeze-bonds between ice blocks

- Dimension and orientation of ice blocks

- Strength of submerged ice in the ice-keel

and also three mechanisms for when ice rubble deforms

- Failure of the freeze-bonds

- Rotation and rearrangement of the ice blocks

- Failure of the ice blocks themselves

The load exerted by a ridge depends on different external parameters as geometry and ice drift, and internal parameters as the internal structure of the ridge and its mechanical characteristics [Shafrova and Høyland, 2008]. The parameters that influence the rubble strength have been discussed in many scientific papers. Confinement pressure, strain-rate, size of ice blocks, void ratio, time history are parameters suggested by Liferov and Bonnemaire [2005]. Also the initial ice-block temperature, salinity, consolidation time and the surrounding oceanic flux have been studied. The parameters directly influencing the freeze-bond strength will be presented in section 2.3.

2.2   Former freeze-bond investigations

Experimental investigations on freeze-bonds have been conducted both in the field and the larger part in the laboratory. Most of the investigation is done on the topic of freeze-bond strength and the parameters influencing it. Some research have also been conducted studying the freeze-bond growth and its thermal development.

Artificial freeze-bonds have been formed by placing two ice pieces together with a known distance or pushed together with a predefined pressure (normal confinement). The ice blocks are then placed in air or submerged in water for a given amount of time where the freeze-bonds are formed. Fresh, saline and sea water have been used for submersion.

The main parameters previously investigated is the relation between the freeze-bond strength (τ_{fb}) and the submersion time (Δt), confinement pressure (σ), initial ice temperature (T_i), velocity of compressing piston (v), sample volume (V), contact area (A) and contact surface.
The freeze-bond strength has been defined as the maximum measured shear force (independent of confinement).

Three methods of measuring the freeze-bond strength has been used. A principal sketch is shown in figure 2.2
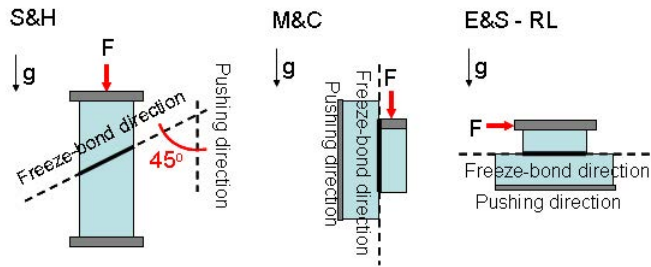
Figure 2.2: Illustration of experimental set-up from Repetto-Llamazares et al. [2011a]. S&H-Shafrova and Høyland [2008], M&C- Marchenko and Chenot [2009], E&S- Ettema and Schaefer [1986], RL- Repetto-Llamazares et al. [2011b]

Ettema and Schaefer [1986], Repetto-Llamazares et al. [2011b], Repetto-Llamazares et al. [2011a], Helgøy [2012] and Astrup [2012] used the test set-up where two ice blocks are placed on top of each other, the lower block is kept in a fixed position while a horizontal force is applied to the upper block. Marchenko and Chenot [2009] applied a similar set-up, only vertically oriented on relation to the freeze-bond and the applied force. Shafrova and Høyland [2008] and Møllegaard [2012] used the set-up where the freeze-bond is aligned at 45° relative to the applied piston force and the edges. In these tests a cylindrical ice sample was used and cut by band saw to create the surfaces. All the above mentioned experiments used a set-up where there is direct contact between the ice blocks when the freeze-bonds are formed. And the freeze-bond strength is defined from the Mohr-Coulomb failure criterion. This criterion applies cohesion (c) and the angle of internal friction (ϕ) as material properties, while the normal stress (σ) is defined from the boundary conditions. The material properties define a failure surface in the τ-σ space, so that for a specific normal stress a freeze-bond shear strength is defined.

2.3   Parameters influencing freeze-bond strength

The dependence of freeze-bond strength (τ_{fb}) on several physical properties have been investigated in several experiments and reviewed. A summary of the findings from tests preformed on freeze-bonds submerged in water will be presented in this section.

2.3.1   Submersion time Δt

This parameter was first tested by Ettema and Schaefer [1986]. They applied relatively short submersion times from 10 s to 4 min. For samples submerged in fresh-water an increase in strength with time was found. For samples in 3 % saline water, less increase was observed and for 12.5-25 % saline water no increase was found.

From further experiments a bell-curve has been found to describe the freeze-bond strengths dependency on submersion time. A figure 2.3 first presented in Repetto-Llamazares et al. [2011a], agrees with the predictions of Shafrova and Høyland [2008].
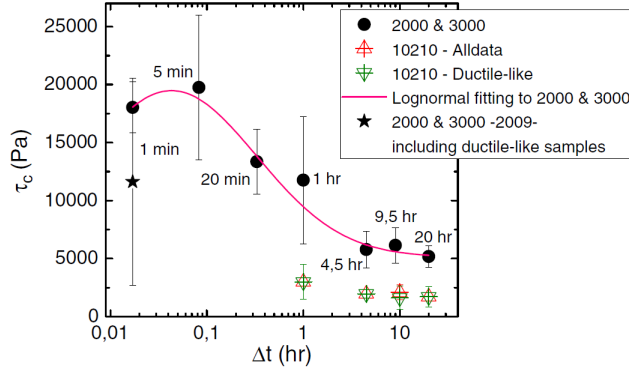
Figure 2.3: Freeze-bond shear strength vs. submersion time from Repetto-Llamazares et al. [2011a]

The freeze-bond strength was tested with submersion times of [1, 5, 20]min and [1, 4.5, 9.5, 20]hours. Increasing strengths was found up to 20 min, beyond this point the strength started to decrease. It is proposed that the strength development under submersion is a development of the porosity. It was suggested that three phases may be applied to describe this observed development. The first phase is defined as where the freeze-bond temperature decrease and the strength increase towards a maximum. This phase ends and the second starts when the freeze-bond temperature and the brine salinity is in equilibrium with the surrounding ice. This is the point when both the temperature and the porosity is at it's lowest point. In the second phase the temperature rises again and the brine drains, which is assumed to affect the freeze-bond porosity. The brine will normally drain slower than the temperature rises, this leads to a total increase of the porosity and a decreasing strength. The third phase starts when there are no more gradients, the salinity and temperature of the freeze-bond is in equilibrium with the surrounding water, and the processes slows down and

stabilizes. The temporal development of the strength is well illustrated by Shafrova and Høyland [2008] for sea ice strength (σ_{si}) and freeze-bond strength of both fresh ice (σ_{fb}(fresh ice)) and sea ice (σ_{fb}(sea ice)) shown in figure 2.4.
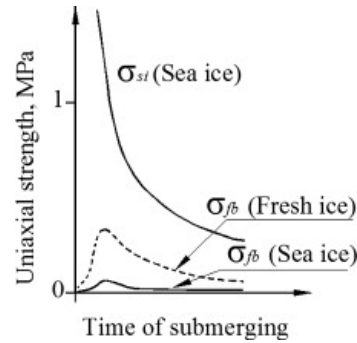
Figure 2.4: Idealized strength development over time from Shafrova and Høyland [2008]

2.3.2 Confinement pressure σ

Several sets of experiments have been conducted to determine the freeze-bond strength dependency on confinement pressure and several configurations have been used. The "classical" configuration of experiments is applying the same pressure during submersion and during testing. An "inverse" configuration is where one uses a high pressure during submersion and low during testing, or the other way around.

Ettema and Schaefer [1986] used the classical configuration and measured increasing freeze-bond strength with increasing confinement. These tests were conducted with a submersion time of 10 seconds. The increase was 6 to 10 times larger when submerged in fresh-water than for 12.5 to 25 % saline water. Repetto-Llamazares et al. [2011a] applied both the classical and inverse configuration when investigating confinement pressure. They used a submersion time of 20 hours. An illustration of the experimental procedure is shown in figure 2.5.
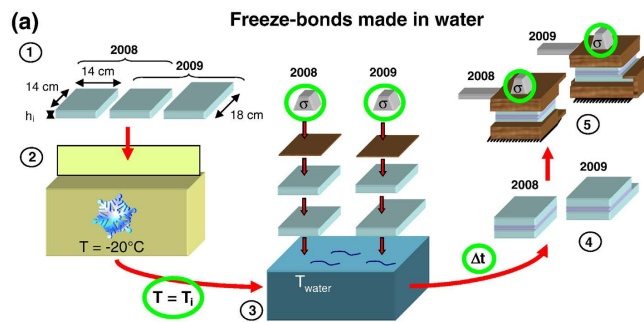
Figure 2.5: Illustration of experimental set-up used by Repetto-Llamazares et al. [2011a]

Several confinement pressures were used in the experiments; [25, 125, 147, 170, 295, 637, 650, 660, 1075, 1205, 2000, 2040]pa. Overall increasing strengths (τ_{fb}) with increasing normal pressure(σ) was measured. A Mohr-Coulomb failure criterion was therefore applied to describe this relation, see equation 2.2, and material properties for cohesion (c) and internal friction angle (ϕ) were found. By extrapolating the results it was also shown that the measurements were corresponding with those done by Shafrova and Høyland [2008].

$$\tau = \sigma + tan(\phi) \tag{2.2}$$

2.3.3   Initial ice temperature T_i

Shafrova and Høyland [2008] found that in general the strengths of both the ice and the freeze-bonds decreased for increasing initial temperature and porosity, also partly for increasing salinity. The correlation between the freeze-bond strength and the initial temperature was found to be particularly strong, changes of 1-2 °C was measured to have an effect on the strength.

Repetto-Llamazares et al. [2011a] found a clear trend only for the tests with low confinement. It was measured an increasing freeze-bond strength with increasing initial temperature, which is the opposite of what was found by Shafrova and Høyland [2008]. The initial ice temperature can affect the freeze-bond in two ways. Very low temperatures give more energy so that the freeze-bond form more quickly. At the same time it can cause weaker, more porous ice by that more brine is trapped. This phenomenon may have been suppressed by the higher confinement.

The coupling effect between initial temperature and submersion time is discussed by Repetto-Llamazares et al. [2011a]. They concluded that the initial temperature (T_i) have a strong influence for short submersion times (Δt) and is almost insignificant on the freeze-bond strength after a long time, this is shown in figure 2.6. It is suggested that the initial temperature governs the height and width of the bell-curve (figure 2.4) together with the sample size and the thermal properties of the ice.
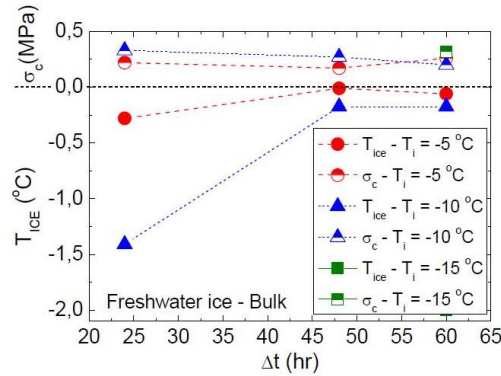

Figure 2.6: Ice temperature and compression strength vs submersion time from Repetto-Llamazares et al. [2011a]

Møllegaard [2012] found results agreeing with stronger freeze-bonds with decreasing temperatures for short submersion times. A transition point was found around 60 min, where the initially coldest ice had the lowest strength. After long submersion times increasing initial temperature gave stronger ice.

2.3.4 Contact surface

The relation between the contact surface properties and the freeze-bond strength was investigated by Helgøy [2012] and Møllegaard [2012]. In the first study, four different combinations of natural top and bottom surfaces of the ice sheet was tested. A difference of 2.2 in strength was measured between the weakest and the strongest combination.

Shafrova and Høyland [2008] and Repetto-Llamazares et al. [2011a] were cut by band saw, while Ettema and Schaefer [1986] used smoothed surfaces. Møllegaard [2012] tested if the surface roughness had an impact on the freeze-bond strength by comparing smoothed surfaces to those cut by a band saw. He found no difference between the two.

2.3.5 Physical properties of the ice; salinity, porosity, block size and structure

The correlation between initial salinity and freeze-bond strength was discussed by Shafrova and Høyland [2008]. From the laboratory tests the freeze-bond strength was measured to be 5-10 times higher for fresh water than for saline ice. A trend of decreasing strength with increasing salinity up to 3ppt was observed. For higher salinities it is discussed that the brine volume is more sensitive to temperature variations. A transition point where the effect of small temperature variations becomes larger than that of the total salinity is suggested. Møllegaard [2012] preformed tests with very high salinity (34ppt)of the submersion water and concluded that the strength was considerably lower than for ice submerged in water with a salinity of 8ppt.

Shafrova and Høyland [2008] also found a freeze-bond strength dependency on porosity. A higher ice fraction contains more potential energy that can be spent creating freeze-bonds. High air volume and low brine volume is found to have two effects; high thermal conductivity, which slows down the temperature diffusion and the higher air volume increases the mass diffusion.

Repetto-Llamazares et al. [2011a] found that the sample size is important in at least two ways. The A/Vol ratio determines the available energy to create freeze-bonds, a larger volume gives higher available energy. Shafrova and Høyland [2008] found that the strength of small blocks were lower than the average strength of large blocks. Which agrees with that a lower A/Vol ratio gives stronger freeze-bonds. The second influencing factor was shown by Strub-Klein et al. [2010], where the importance of drainage along the freeze-bond plane was pointed out. Shafrova and Høyland [2008] measured weaker freeze-bonds in the interior of an ice block than from the exterior, which implies that a small contact area may create stronger freeze-bonds. Møllegaard [2012] found the same trend as Shafrova and Høyland [2008]. Experiments on salinity variations in the freeze-bond plane was conducted together with measurements of the temperature evolution. No salinity variations was found. The temperature in the center of the ice block reached its minimum after two

hours, much later than expected, which can explain the variation in strength throughout the plane.

The growth texture of the ice influences it's strength. Texture is here used to define the preferred orientation of grains within poly-crystals. The digits 1, 2 and 3 are used to describe the orientation. S1 meaning a secondary ice where the c-axis is dominant in the vertical direction. for S2 the c-axis is dominant in the horizontal plane and is randomly oriented within this plane. S3 denotes ice where the c-axis is dominant in the horizontal plane and is aligned in a particular direction in this plane. This definition is based on that from Schulson et al. [2009].

2.3.6 Piston velocity

The effect of the piston velocity on the freeze-bond strength have been investigated by Ettema and Schaefer [1986] and Astrup [2012]. Piston velocities of [0.44, 0.84]mm/s and [1, 10m]m/s were used in the experiments respectively. The measured strengths showed no dependency on the piston velocity.

2.4   Calculations

2.4.1   Freeze-bond shear strength τ_{FB}

$$A_{ellips} = \sqrt{2}\pi r^2 \tag{2.3}$$

$$A_{circ} = 2\pi r^2 \tag{2.4}$$

$$h = \frac{2r}{\pi}\theta \tag{2.5}$$

$$\sigma_z = \frac{Measured piston force}{A_{circ}} \tag{2.6}$$

Force from σ_r in x-direction:

$$
\begin{aligned}
F &= -2\int_0^\pi \sigma_r h(\theta) r\cos(\theta)d\theta \\
&= -2\sigma_r\frac{2r}{\pi}r\int_0^\pi \theta\cos(\theta)d\theta \\
&= -K[\pi*0+\cos\pi-(0*0+\cos0)] \\
&= -K[+(-1)-(1)=2K \\
&= 8\sigma_r\frac{r^2}{\pi}
\end{aligned}
\tag{2.7}
$$

Sum of forces in z-direction:

$\sum F_z = 0$

$$
\begin{aligned}
\sigma_z\pi r^2 - \frac{\sqrt{2}}{2}\tau_{FB}\sqrt{2}\pi r^2 - \sigma_{FB}\frac{\sqrt{2}}{2}\sqrt{2}\pi r^2 &= 0 \\
\sigma_z - \tau_{FB}\sigma_{FB} &= 0 \\
\tau_{FB} &= \sigma_z - \sigma_{FB}
\end{aligned}
\tag{2.8}
$$

Sum of forces in x-direction:

$$\sum F_x = 0$$

$$8\sigma_r \frac{r^2}{\pi} + \frac{\sqrt{2}}{2}\tau_{FB}\sqrt{2}\pi r^2 - \frac{\sqrt{2}}{2}\sigma_{FB}\sqrt{2}\pi r^2 = 0$$

$$\frac{8}{\pi}\sigma_r + \pi\tau_{FB} - \pi\sigma_{FB} = 0 \tag{2.9}$$

$$\sigma_{FB} = \frac{8}{\pi^2}\sigma_r + \tau_{FB}$$

Equation 2.8 in equation 2.9

$$\sigma_{FB} = \frac{8}{\pi^2}\sigma_r + \sigma_z - \sigma_{FB}$$

$$= \frac{4}{\pi^2}\sigma_r + \frac{1}{2}\sigma_z$$

$$\tag{2.10}$$

$$\tau_{FB} = \sigma_z - \frac{4}{\pi^2}\sigma_r - \frac{1}{2}\sigma_z$$

$$= \frac{1}{2}\sigma_z - \frac{4}{\pi^2}\sigma_r$$

2.4.2 Strength parameters, cohesion and internal friction coefficients

To estimate the cohesion and internal friction coefficients a least squares approach have been used to draw a linear failure slope through the measured shear stress - compression stress points.

The least squares approachis a mathematical procedure to find the best fitted curve through a set of datapoints by minimizing the offsets between each point and the curve. For these experiments a linear curve was chosen.

Linear least squares

First degree polynomial with unknowns k_1 and k_2

$$y = xk_1 + k_2 \tag{2.11}$$

To solve this equation one can use a system of n simultanious linear equations in two unkowns.

$$S = \sum_{i=1}^{n}(y_i - (x_i k_1 + k_2))^2 \tag{2.12}$$

The fitting minimizes the summed square of the residuals, which means that the coefficients are determined by differentiating S with respect to each parameter and setting them equal to zero.

$$\frac{\delta S}{\delta k_1} = -2 \sum_{i=1}^{n} x_i(y_i - (x_i k_1 + k_2)) = 0 \tag{2.13}$$

$$\frac{\delta S}{\delta k_2} = -2 \sum_{i=1}^{n} (y_i - (x_i k_1 + k_2)) = 0 \tag{2.14}$$

Summing from i=1 to n

$$k_1 \sum x_i^2 + k_2 \sum x_i = \sum x_i y_i \tag{2.15}$$

$$k_1 \sum x_i + n k_2 = \sum y_i \tag{2.16}$$

Solving for k_1

$$\frac{n \sum x_i y_i - \sum x_i \sum y_i}{n \sum x_i^2 - (\sum x_i)^2} \tag{2.17}$$

Solving for k_2 by k_1

$$\frac{1}{n} (\sum y_i - k_1 \sum x_i) \tag{2.18}$$

Mohr-Coulomb failure criterion

A mathematical model describing the response of brittle materials to shear and normal stress.

$$\tau = \sigma + tan(\phi) \tag{2.19}$$

where τ is the shear strength, σ is the normal stress and c is the intercept of the failure envelope with the τ-axis, often denoted as the cohesion. ϕ is the slope of the failure envelope and is denoted the angle of internal friction.
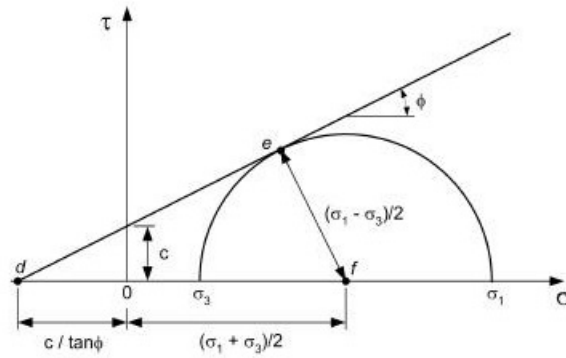

Figure 2.7: Mohr's circle of stress

where σ_1 denotes the maximum principal stress direction, σ_2 is the intermediate principal stress direction and σ_3 is the minimum. In this thesis $\sigma_2 = \sigma_3$ and are denoted σ_r.

Chapter 3

Experimental method

Shear strength measurements of laboratory made freeze-bonds have been investigated in the Cold Lab at UNIS. Both uni-axial tests without confinement and tri-axial tests (radial confinement and compression along one axis) have been conducted. The uni-axial test set-up is based upon experiments by Shafrova and Høyland [2008] and Møllegaard [2012]. Further the tri-axial tests have been conducted within the same parameters.

Five uni-axial tests have been conducted on fresh ice and eight on saline ice to compare with the results of Møllegaard [2012]. For both types of ice, 12 test configurations have been chosen for the, resulting in 24 in total, to be tested with three different confinements. A total of 60 samples was presented of those who were tested in the pressure clock. These tests have been conducted in the period from January to April 2014 in the Cold Lab at UNIS.

3.1   Ice production and properties

Both saline and fresh water was used in these tests. The saline ice was produced in the ice production basin FRYSIS. This production basin have heated walls and bottom to induce ice-growth from above. It has a surface area of 1000 x 500 mm and a depth of 1250 mm, a total volume of 625 litres. Three ice sheets were produced (Sheet1, Sheet2, Sheet3) from water of approximately 8ppt, which gave in total 61 samples. A method of growing ice by seeding the surface with small water droplets was used. This method is based on the article of Helgøy [2013]. A fully developed S1 ice with smaller grains than observed for ice grown from a free water surface was found by using this method. 1-2 cm ice was grown in the tank, then removed to give a free surface, then a spray-bottle was used to seed the ice with small water droplets. Figure 3.1 shows Sheet 1 and 2, which was produced at a temperature of -15°C. And Sheet 3 was produced at -20°C to increase the growth process.

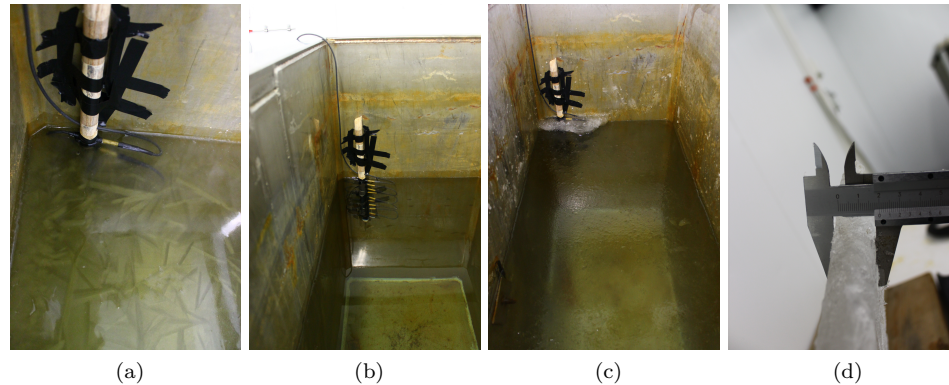| | | | |
| (a) | (b) | (c) | (d) |

Figure 3.1: a) Before seeding of the ice b) the tank after a 2cm layer of ice has been removed c) after the seeding d) a sample of the 2cm ice that was removed

It was attempted to grow fresh water ice in the same manner as the saline ice. Because of no air bubbles/brine pockets, pressure was built up under the ice, to the point where the growth process stopped. The fresh water ice used in the tests are collected from Isdammen in Longyearbyen over a two day period in January. A total of 50 samples was collected by using a 70 mm ice core sampler, kovacs.

Both the saline and fresh water samples was cut to the appropriate length, sealed in plastic bags and placed in storage at -18°C in a Zarges box. The 45° section where the freeze-bond is grown were cut just before testing.

The ice properties of the three lab made sheets and the fresh water samples are given in table 3.1.

3.1.1   Thin-sections

Saline ice samples

Thin-sections were used to study the ice texture of the fresh water ice and the three ice sheets formed in the FRYSIS tank. A microtom was used to plane the samples down to a thickness of approximately 0.4 mm. Pictures were then taken through a polaroscope.

For all three ice sheets the structure was found to be in-between S1 and S3 ice (Defined in chapter 2.3.5). The core samples from the middle had a S1 structure, while the samples taken closest to the walls can be described as laying between S1 and S3 structure. During the growth process the heaters of the walls was observed to have a lower temperature than expected. This suggests that there was a heat-flux not only from the top but from the walls as well. This coincides with was is seen in the structure of the ice. Figure 3.2 to 3.4 shows a selection of thin-sections from each ice sheet.

Figure 3.2: Thin-sections of ice sheet 1, sample taken approxiamately 15cm from the wall of the tank. To the left horizontal sections, upper 2-4cm from the top and bottom section 13-15cm from the top. To the right vertical sections, upper 0-5cm from the top and bottom section 5-10cm from the top.
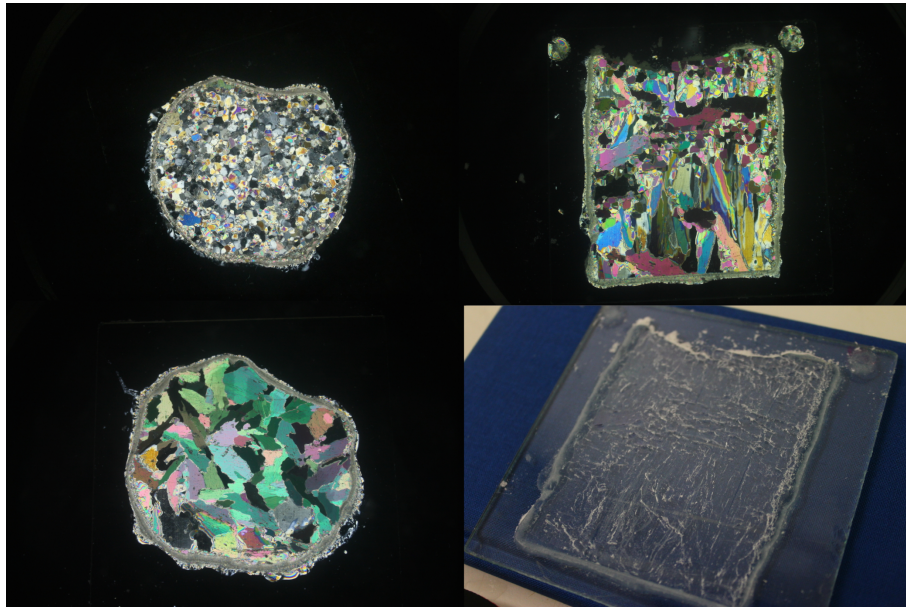
Figure 3.3: Thin-sections of ice sheet 2, sample taken approximately 15cm from the wall of the tank. To the left horizontal sections, upper 2-4cm from the top and bottom section 14-15cm from the top. To the right vertical sections, upper 4-12cm from the top and bottom picture shows the same vertical section without polarized glass.
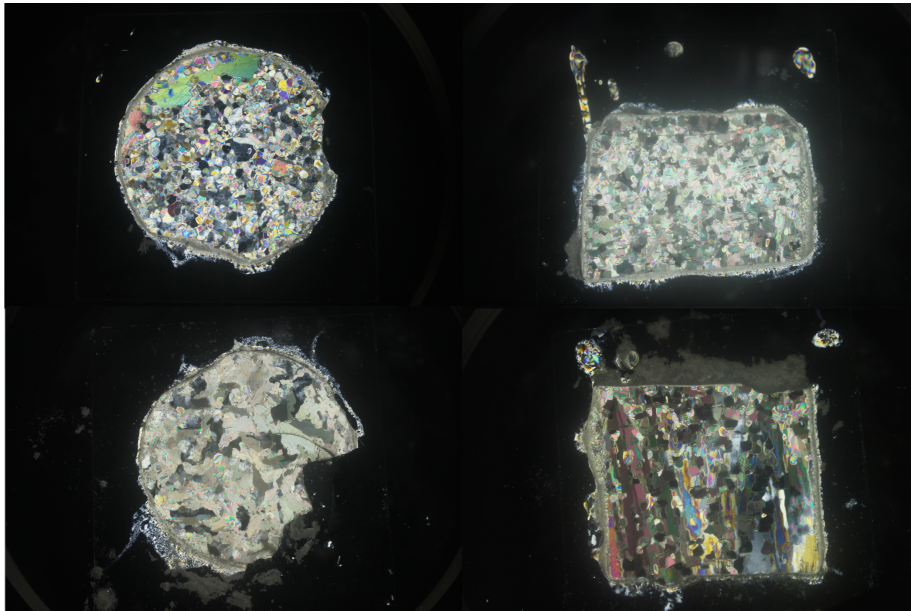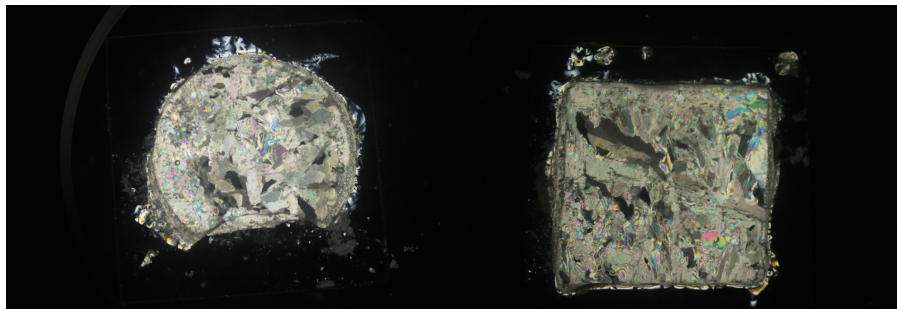

Figure 3.4: Thin-sections of ice sheet 3, sample taken approximately 5cm from the wall of the tank. To the left horizontal section at depth 15-17cm and to the right vertical section at depth 10-15cm.

Fresh water samples

The fresh water samples collected from Isdammen were found to have a columnar structure, defined as S1 ice. Figure 3.5 shows some selected thin-sections. From the horizontal section it can be seen that the average grain size is 90 mm.

The vertical sample at the top shows a surface structure deviating from the otherwise columnar structure seen in the lower vertical thin-section.
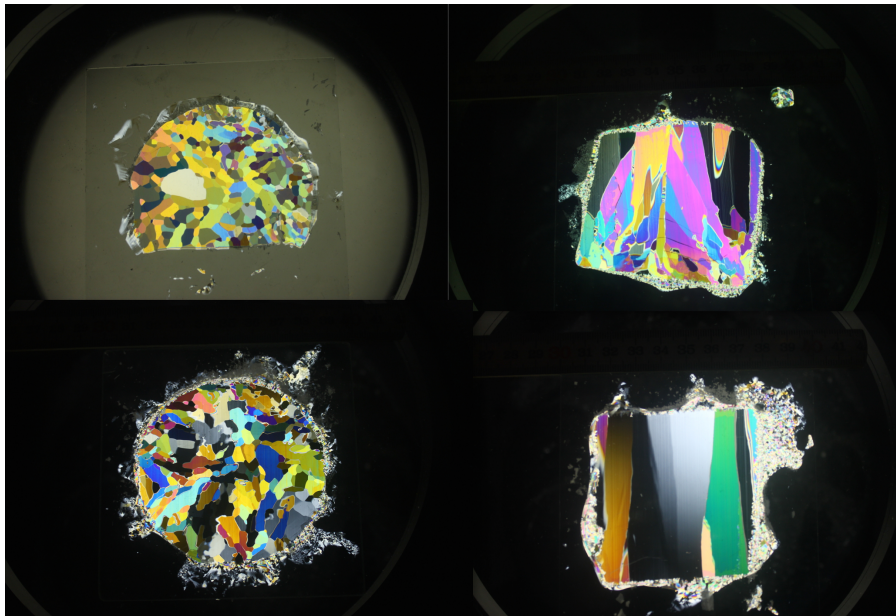
Figure 3.5: Thin-sections of fresh water sample from Isdammen. To the left horizontal sections, upper 3-5 cm from the top and bottom section 17-19 cm from the top. To the right vertical sections, upper 0-5 cm from the top and bottom section 10-15 cm from the top.

The samples from Isdammen had a varying density. This could be observed by the degree and size of the air content. Figure 3.6 shows three fresh water samples with different air contents. The calculated density of these samples varied between $920.5 kg/m^3$ and $941.4 kg/m^3$. Shafrova and Høyland [2008] found that the freeze.bond strength depends on porosity. A sample with higher ice fraction contains more potential energy that can be spent creating freeze-bonds. High air volume and low brine volume was found to have two effects; high thermal conductivity, which slows down temperature diffusion, and it increases the mass diffusion.

Table 3.1: Ice properties

	Sheet1	Sheet2	Sheet3	Fresh water
Number of samples	20	20	21	50
Production temperature	-15	-15	-20	variable
Salinity water [ppt]	7.75	8.06	7.98	0.43
Salinity ice [ppt]	2.25	2.27	2.76	X
Initial thickness [mm]	2	47	877	~1500
Ice texture	S1/S3	S1/S3	S1/S3	S1
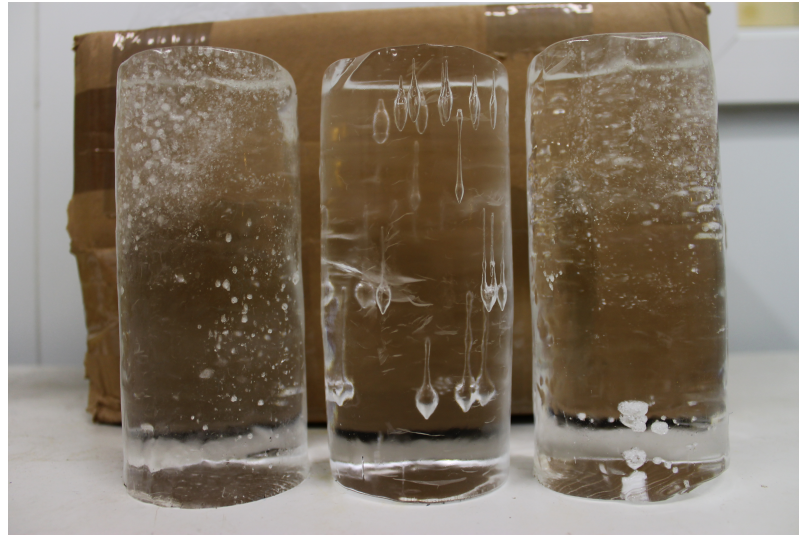
Figure 3.6: From the left; samples with small, large and intermediate bubbles.

3.2 Test procedure

To prepare for the tests the pre-cut samples were taken out of the freezers and placed in the Cold Lab until the ice was in thermal equilibrium with the air temperature, which was set to the desired initial temperature (T_i). The basin used to submerge the samples were also placed in the lab and continuously stirred until the desired temperature (T_w) was reached.

Firstly the dimensions of a sample was measured and logged before a 45° section was cut with a circular saw as shown in figure 3.7a. Secondly the sample was assembled again by installing the two pieces in the FIXIS device, seen in figure 3.7b. This was then immediately placed in the basin and submerged for a given time (Δt)(figure 3.7c). The samples were submerged without any confinement, except that of the water. The salinity (S_w) and the temperature (T_w) of the submersion

water was measured between each sample. After submersion the sample was removed from the FIXIS and placed in the pressure-clock, which again was placed in the KNEKKIS machine. The pressure in the clock was then set to the desired value (σ_r) before the piston force was applied with a constant velocity (V) of 48mm/min.

The deformation limit was constrained by the height of the pressure-clock, this sets the limit to 17-20mm. During compression of the sample a valve adjusts the pressure in the clock so that it was kept at the set value. Deformation (Δh) and piston force (σ_z) was logged and saved at a minimum of every 0,1 seconds. After the test the temperature of the sample ($T_{ice,test}$) was measured (figure 3.7d), the failure mode was written down together with relevant comments and pictures were taken. The sample was then placed in a small container to melt and later measure the salinity.
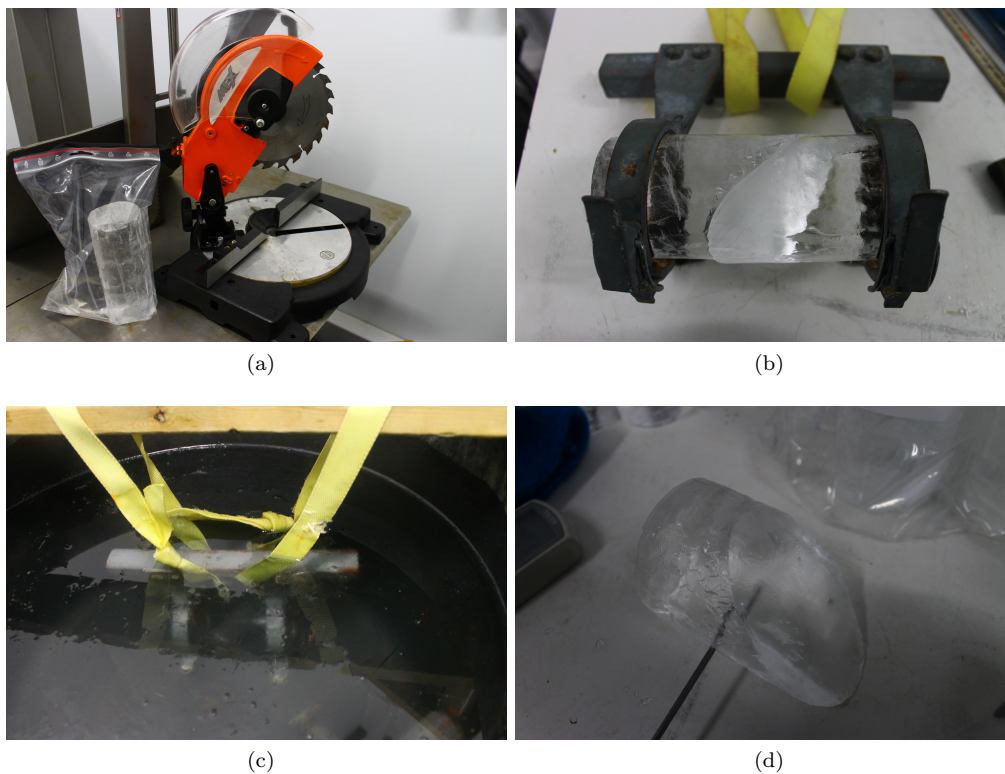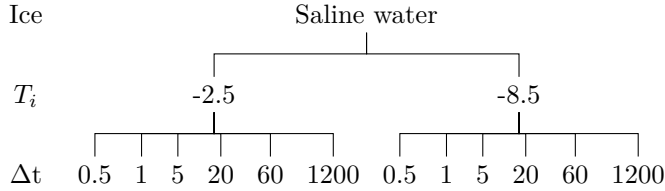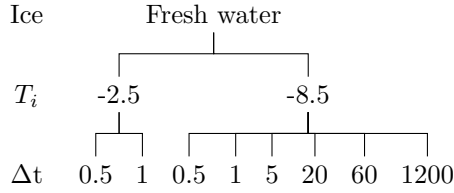

Figure 3.7: a) Circular saw used to cut 45° section b) FIXIS with installed sample c) submerged sample in basin d) temperature measurement after compression

3.3   Test configurations

Four test series were conducted, two with fresh water ice submerged in fresh water (denoted FT) and two with saline ice submerged in saline water (denoted ST). Each test series were divided into six configurations, where all was tested with three pressure values for σ_r. one exemption was for the fresh water samples with initial temperature of -2.5° which inly was tested for the two shortest submersion times. This because of very weak freeze-bonds beyond this point. The test matrix is illustrated below. For each submersion time three samples were tested, each with a different confinement σ_r, which is listed in 3.1. The actual number of samples is presented in appendix A.

```
Ice            Fresh water
             ┌───────┴───────┐
T_i      -2.5              -8.5
          ┌┴┐         ┌──┬──┼──┬───┐
Δt      0.5  1      0.5  1  5  20 60 1200
```

```
Ice                    Saline water
                 ┌──────────┴──────────┐
T_i            -2.5                   -8.5
       ┌──┬──┬──┼──┬───┐     ┌──┬──┬──┼──┬───┐
Δt    0.5  1  5  20 60 1200 0.5  1  5  20 60 1200
```

$$\sigma_r = [0.0070 - 0.0094, 0.0200 - 0.0212, 0.0987 - 0.1026] MPa \tag{3.1}$$

As illustrated in the matrix two values were chosen for the initial temperature of the ice, [-2.5, -8.5]°C, and six different submersion times were used, [0.5, 1, 5, 20, 60, 1200]min. These were chosen on the basis of uni-axial tests previously conducted by Shafrova and Høyland [2008] and Møllegaard [2012]. In addition uni-axial tests were conducted to compare the reproducibility and thus the comparability of the mentioned tests. Both saline and fresh water samples were tested. The initial temperature was set to -8.5°C and the strength was tested for submersion times of [0.5, 1, 5, 20]min.
The air temperature was set to the same value as the initial ice temperature for both the uni-axial and tri-axial experiments.

The temperature of the submersion water T_w was set according to the freezing point of the water, -0.5°C for 8ppt and 0.0°C for fresh water. The saline water was mixed from approximately 1/4

ocean water and 3/4 spring water. The fresh water was taken from the spring which is tapped from Isdammen. The salinity measurement of the submersion water was done when it was mixed (room tempered water) as well as during testing (cold water). A small difference was seen in the measurements when the water was cooled down, which could not be explained by the expulsion of salt or sinking of salter water. This indicated that the salinity-meter may be sensitive to large temperature differences or to cold water.

The dimensions of the samples were forced by the devices used, the hight of the sample was forced by the dimensions of the pressure clock and the diameter of 70 mm was given by the core sampler kovacs. The samples are therefore 150 mm in hight instead of 175 mm, which has been more often used in previous studies.

3.4   Freeze-bond strength measurement

The freeze-bond strength measurements was conducted by using the compression machine KNEKKIS. For these tests the cylindrical samples were compressed in a vertical direction (in the growth direction) with a constant velocity by the piston. The samples were compressed vertically with a 45° angle on the freeze-bond. This piston is connected to a load cell, which is again connected to a computer where the measurements were logged continuously during testing. The distance from the piston and the top of the core sample was manually adjusted before the test to be as small as possible. Deformation was also logged and measured between the piston and the bottom steel plate. The log time was set to a minimum of 0.1 seconds.

The radial pressure was obtain by using a pressure clock previously used for soil and snow. This was connected to a pressure valve, which again was connected to a pressure measurement device and pump. The valve had a range from 0.7 kPa to 400 kPa. During testing the range with which the radial pressure varied was manually logged.

With a 45° compression angle relative to the freeze-bond a shear fracture resulting from displacement along this plane is obtained. This angle also gives the highest shear stress in the freeze-bond. How the internal forces are calculated was presented in chapter 2.4.1.

The KNEKKIS machine was used by both Møllegaard [2012] and Shafrova and Høyland [2008] , which ensures that there is little calibration difference.

3.5   Measured variables

In addition to force measurements several variables were measured before and after the experiments. In appendix A all measured variables are listed for each sample.

Before each test series the core temperature of a reference sample, which had been placed together with the other samples, was measured. This to ensure that the wanted initial temperature was in the desired range. The dimensions of each sample, the temperature T_w and the salinity S_w of the

submersion water was measured before each sample was tested. For the longest submersion time of 1200 min some ice was removed from the surface of the submersion tank and the temperature was measured occasionally.

The core temperature of the ice after testing was measured for each sample. The temperature was measured approximately at the center of the sample and for most samples the core temperature was also measured at the bottom or top of the sample. The failure mode was determined and pictures were taken when the sample was taken out of the pressure clock. The salinity S_i of the sample was measured the day after testing.

The surface roughness was not evaluated, but using the definition of Møllegaard [2012] it would be defined as a rough surface. It was concluded in that thesis that the smoothness of the surface had no effect on the freeze-bond strength.

3.6   Thin-sections of freeze-bonds

Thin-sections of compressed samples were conducted on a small selection. In total 8 thin-sections were prepared. Table 3.2 presents the samples used for thin-sections and their test configurations. A picture of each sample is presented in appendix E.

Table 3.2: Freeze-bond thin-sections

	FT-21	FT-22	ST-1	ST-2	ST-4	ST-10	ST-16	ST- 28
T_i	-8.5	-8.5	-2.5	-2.5	-2.5	-2.5	-2.5	-8.5
Δt	5	20	0.5	1	20	20	20	20
σ_r	0.099	0.099	0.007	0.007	0.007	0.020	0.099	0.020
Figure nr	E.1a	E.1b	E.1c	E.1d	E.1e	E.1f	E.1g	E.1h

The tested samples were placed in plastic bags and stored at a temperature of $-10°$C. A vertical section was cut out in the middle of the sample, approximately parallel to the $45°$ angle of the freeze-bond. An example is shown in figure 3.8.
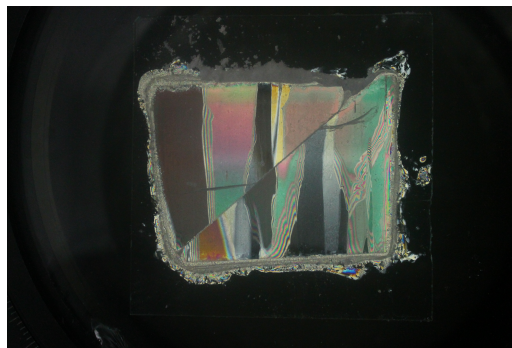

Figure 3.8: Example of a freeze-bond thin-section, FT-21

Chapter 4

Results

4.1 Introduction

In this chapter the results and observations from the experiments are presented. Firstly the failure modes and observed fracture behaviour is presented. Following is a section presenting the results of freeze-bond stresses. This section is divided into sub-sections where the stress is presented in relation to the chosen variables of the experiments.

The freeze-bond strength has been defined as the maximum measured shear force and the freeze-bond stress as the strength divided by the contact area ($A_{ellipse}$). The contact area has not been adjusted according to the decreasing nominal area during testing. This because the main focus has been on the peak force, occurring before any major deformation have taken place. Primarily the peak freeze-bond stress has been used to present the results.

In appendix A the full freeze-bond experiment dataset is presented. In appendix B and C figures of the failure slopes are presented for all configurations, for peak stresses and residual stresses accordingly. This will be explained further in section 4.3.2. In appendix D all estimated cohesion and internal friction values are presented for each configuration both for peak and residual stresses. This will be presented in depth in chapter 4.3.3 *Cohesion and internal friction angles*.

26

4.2 Failure modes ductile or brittle

The slope of the shear force - time curve just after failure was investigated for each sample to distinguish the failure mode, ductile- vs brittle-like. In the two sub-sections 4.2.1 and 4.2.2 the visually observed fracture behaviour was presented.

The failure mode was determined by visual observations of the plots and the steepness of the unloading slope. In table 4.1 the failure mode, the average, maximum and minimum value of the unloading slope are presented for each test segment. The uncertainty in S_{avg} was taken as $\pm$ one standard deviation. In this table it was not distinguished between freeze-bond failure and a combined failure of sliding along the freeze-bond and crushing at an edge (figure 4.2 d), this only applied for two fresh water samples at the initial temperature of -2.5°C.
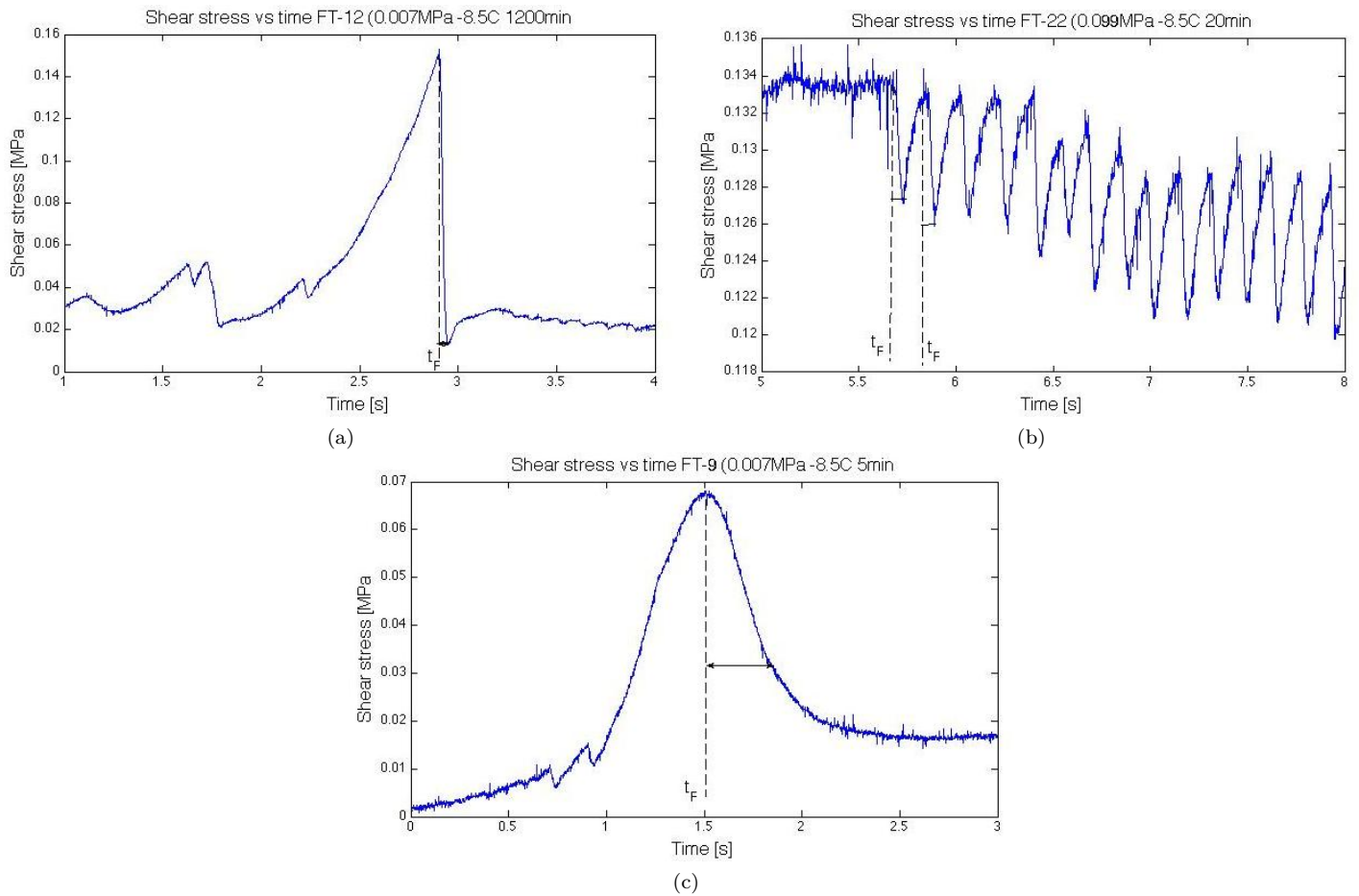

Figure 4.1: Representative time [s] vs shear stress plots [MPa]. a) FT-12 Brittle failure (0.007 MPa, -8.5°C, 1200 min) b) FT-22 Continues brittle failure (0.099 MPa -8.5°C, 20 min) c) FT-9 Ductile failure (0.007 MPa -8.5°C, 5min)

The brittle failure mode consisted of two phenomenons, the first where the freeze-bond loosed almost all it's strength directly after failure (4.1 a) and the second where after the first failure the pressure built up and failed again, creating a series of peak loads and subsequent failures (4.1 b). The last type of failure was distinctive for the fresh water ice and was not observed for any of the saline tests.

The brittle failure mode was most often observed for shorter submersion times for both the saline and fresh water samples. For a few cases the samples failed brittle-like up to the submersion time of 60 min, but this was not the norm. And equally the ductile failure mode was observed to occur at the longer submersion times, but also here an exception of one sample failing ductile-like for a submersion time of 0.5 min and the initial temperature of -2.5°C. All ductile samples were found to have a comparatively low stress.

The steepness of the unloading slope S_{avg} was observed to be dependent on initial temperature. At the lower temperature S_{avg} decreased faster for both the saline and fresh water samples. The highest decrease in S_{max} was found for a fresh water sample at -8.5°C with submersion time of 1 min. From table 4.1 it was evident that the fresh samples had a larger effect of the temperature difference than for the saline.

Table 4.1: Failure mode, initial temperature (T_i) and unloading slope (S).
Number of samples N, ratio of samples, average unloading S_{avg}, maximum unloading S_{max} and minimum unloading S_{min}.

	Failure mode	N	%	S_{avg} [MPa/s]	S_{max}	S_{min}
Fresh water ice -2.5°C	Brittle	6	100	-0.56±0.40	-1.37	-0.21
	Ductile	0	0	-	-	-
Fresh water ice -8.5°C	Brittle	8	50	-3.06±1.54	-5.84	-1.05
	Ductile	8	50	-0.08±0.05	-0.16	-0.02
Saline ice -2.5°C	Brittle	9	56.25	-1.43±1.06	-3.10	-0.32
	Ductile	7	43.75	-0.05±0.03	-0.10	-0.02
Saline ice -8.5°C	Brittle	12	70.59	-1.81±1.05	-3.80	-0.38
	Ductile	5	29.41	-0.03±0.02	-0.07	-0.01

4.2.1   Observed fracture behaviour vs failure mode - Fresh water samples

For the fresh water samples three distinct fracture behaviours could be observed during testing, sliding failure along the freeze-bond, splitting and cracking of the ice. The extent of cracking and splitting varied between the samples.

Below in figure 4.2 representative pictures of the observed fracture behaviours are shown. Fig-

ure 4.3 shows the consecutive shear force - run time plots of the four samples. Each fracture behaviour had a specific force - run time plot, which confirms the observed behaviour, but the difference between crushing of the whole sample or crushing of just an edge combined with sliding was hard to differentiate. The force development was very different for all four samples, but the unloading slope was still steep enough that all of them fall under brittle failure. All the samples failing in a ductile manner was observed to fail by sliding along the freeze-bond.

Samples splitting was observed for submersion times of 0.5 - 1 min and an initial temperature of -8.5°C. While crushing of the samples were only observed for initial temperatures of -2.5°C at 0.5 min submersion time.

(a)   (b)   (c)   (d)
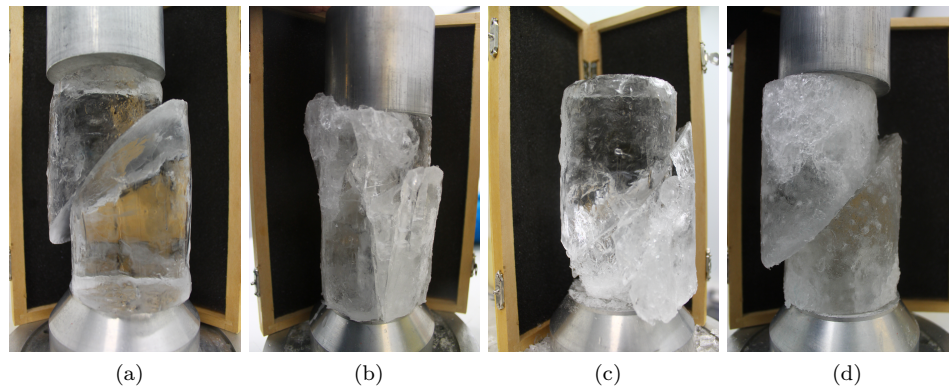
Figure 4.2: a) FT-1 sliding b) FT-13 splitting c) FT-3 crushing d) FT-20 crushing of edge
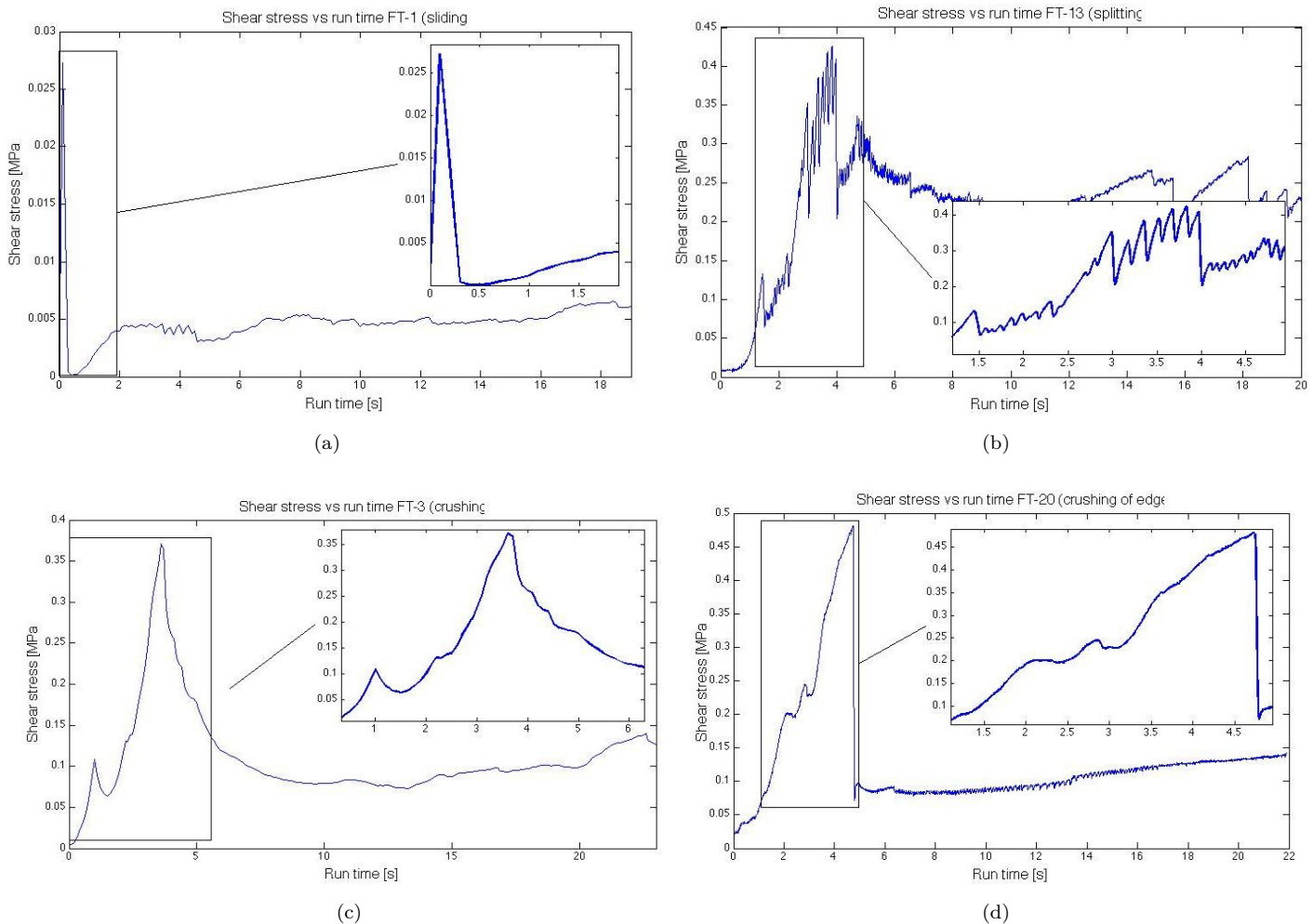
Figure 4.3: Run time [s] vs shear stress [MPa] a) FT-1 sliding b) FT-13 splitting c) FT-3 crushing d) FT-20 crushing of edge

4.2.2   Observed fracture behaviour vs failure mode - Saline water samples

Three fracture behaviours were also observed for the saline samples during testing, but only two samples were observed not to fail by sliding along the freeze-bond. One by crushing, shown in figure 4.4 c), and one by a combination of sliding along the freeze-bond and splitting in the upper part as shown in figure 4.4 d). Figure 4.4 a) and b) shows two representative samples of sliding failure, one in the pressure clock and one after it was removed. The shear force - run time plots are shown

in figure 4.5 for the representative sliding failure and the combination of splitting and sliding. It was possible to recognise the observed fracture behaviour in the plots, a subtle difference between sliding and the combined splitting and sliding could be observed on the loading slope. There was seen no correlation as to why the crushing and splitting failure mode occurred.

Both of the samples presented in figure 4.5 failed in a brittle manner. The same observation as for the fresh water samples was made, all ductile-like samples failed by sliding along the freeze-bond.

(a)　　　　　　(b)　　　　　　(c)　　　　　　(d)

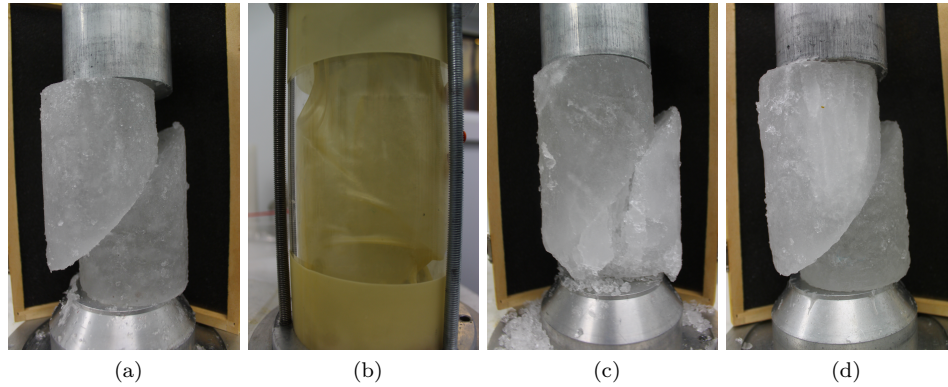Figure 4.4: a) ST-2a sliding b) ST-22 inside pressure clock c) ST-2b crushing of lower part d) ST-32 splitting of edge
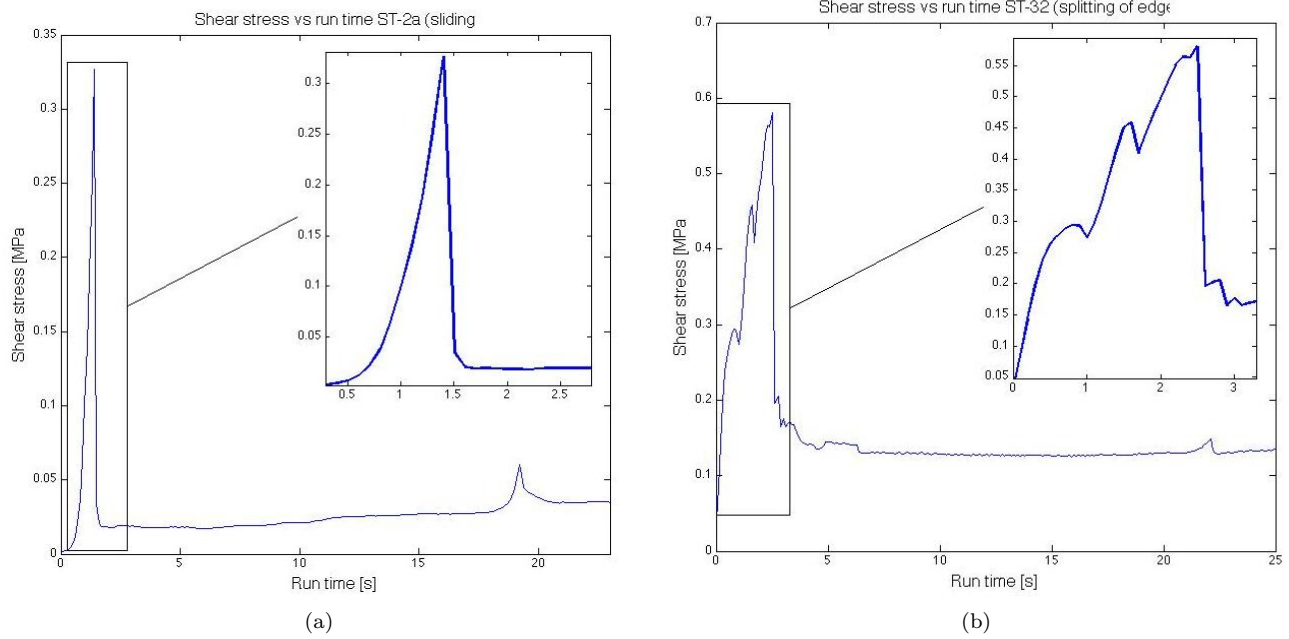
Figure 4.5: Run time [s] vs shear stress [MPa] a) ST-2a sliding b) ST-32 splitting

4.3   Freeze-bond strength

The freeze-bond stress is as previously explained defined as the maximum measured shear force during an experiment divided by the freeze-bonded area. In this section the freeze-bond stress will be studied in correlation with the different chosen variables.

The peak shear stress used in this section is calculated by using the maximum value of the compression stress σ_z in equation 2.10 derived in chapter 2.4.1.

$$\sigma_{FB,max} = \frac{8}{\pi^2}\sigma_r + \sigma_{z,max} - \sigma_{FB}$$
$$= \frac{4}{\pi^2}\sigma_r + \frac{1}{2}\sigma_{z,max}$$

$$\tau_{FB,max} = \sigma_{z,max} - \frac{4}{\pi^2}\sigma_r - \frac{1}{2}\sigma_{z,max}$$
$$= \frac{1}{2}\sigma_{z,max} - \frac{4}{\pi^2}\sigma_r$$

(4.1)

The residual shear stress used is calculated by finding the maximum value of compression and adding 10 saving-steps for the "old" program and 1000 for the new. From this saving-step the mean value of the residual is found. This mean value is then used in equation 2.10 derived in chapter 2.4.1.

$$\sigma_{FB,residual} = \frac{8}{\pi^2}\sigma_r + \sigma_{z,residual} - \sigma_{FB}$$
$$= \frac{4}{\pi^2}\sigma_r + \frac{1}{2}\sigma_{z,residual}$$

$$\tau_{FB,residual} = \sigma_{z,residual} - \frac{4}{\pi^2}\sigma_r - \frac{1}{2}\sigma_{z,residual}$$
$$= \frac{1}{2}\sigma_{z,residual} - \frac{4}{\pi^2}\sigma_r$$

(4.2)

In general the freeze-bond strength was found to be in the same order of 170 - 800kPa. The uni-axial samples were tested for the configurations with initial temperature of -8.5°C and submersion times of 0.5, 1, 5 and 20 min. One sample with hight 175 mm and one for 150 mm were testes for each submersion time. For all submersion times, the shorter sample gave the lower stress, though there was little difference. These experiments were preformed to ensure that the experiments would be comparable.

4.3.1 Confinement σ

Three initial values were chosen for the radial confinement σ_r. In calculations the optimal values were used except for a few samples where they varied largely from the intended value. In table 4.2 the three values are listed together with $\pm$ one standard deviation. The four samples that deviated from the chosen values were not taken into account in the standard deviation and the measured value was used in calculations.

During testing the confinement was logged manually, the start value and the peak value was written down. When the test started the initial confinement was set just under the optimal value (start value) and when pressure was applied in the vertical direction the confinement pressure increased to a peak value, and it kept steady at this value for the duration of the test. The peak value was used for calculating the standard deviations.

Table 4.2: Confinement parameter and standard deviation

	σ_r	σ_{SD}
Confinement$_1$	0.007	± 0.0013
Confinement$_2$	0.020	± 0.0007
Confinement$_3$	0.099	± 0.0017

Peak shear stress

In figure 4.6 and 4.7 the peak shear stress $\tau_{FB,peak}$ is plotted against the peak normal stress $\sigma_{FB,peak}$ for all saline and all fresh samples accordingly. It was separated between initial temperature T_i and confinement (no separation of submersion time Δt, this was presented in 4.3.4).

For the saline samples the lowest initial temperature of -8.5°C had the highest internal stresses, though they vary widely. This was emphasized by table 4.3, where the average peak shear stress over all submersion times is displayed. For the fresh samples the internal stresses were only higher for -8.5°C for the lowest confinement. Important to note here is that only samples for the two shortest submersion times were tested for fresh samples at -2.5°C and only the 4 longest submersion times were used for -2.5°C. This made the comparison between the two initial temperatures T_i intricate.

For both saline and fresh samples the mean peak shear stress $\tau_{FB,peak,mean}$ was generally increasing for increasing confinement. Defined by the peak stress always being higher for the highest confinement than for the lowest. By studying table 4.3 closer, it was seen that the stress-confinement development was not completely linear. For the initial temperature of -2.5°C the intermediate confinement had the highest mean stress. For -8.5°C the intermediate confinement had the lowest mean stress.

The size of the range of the peak shear stresses were calculated (table 4.3), but no correlations
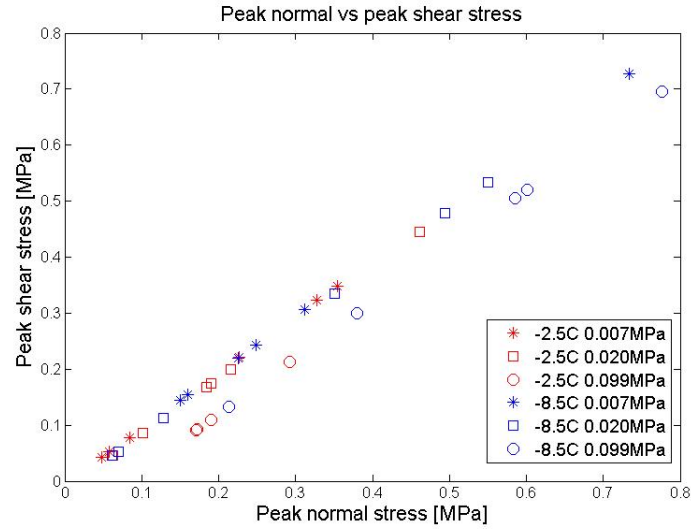
could be seen.

Figure 4.6: Peak normal stress σ_{FB} vs peak shear stress τ_{FB} for three different confinements and two initial temperatures. Saline water samples.
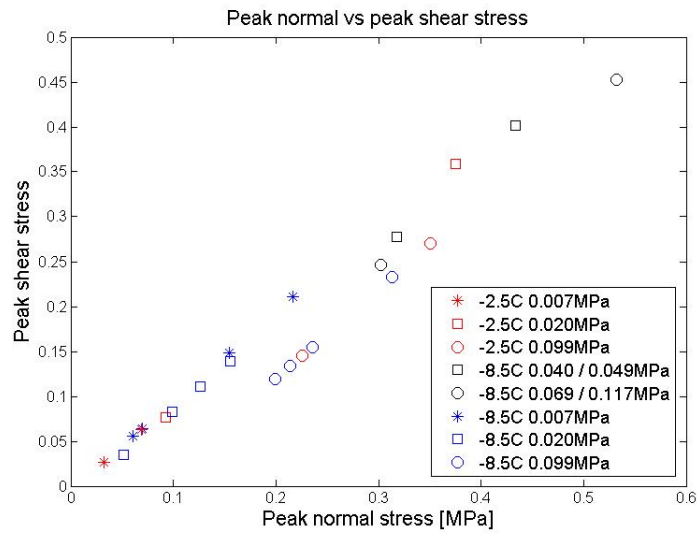

Figure 4.7: Peak normal stress σ_{FB} vs peak shear stress τ_{FB} for three different confinements and two initial temperatures. Fresh water samples.

Table 4.3: Mean peak shear stress $\tau_{FB,peak,mean}$ over all submersion times. T_i gives the initial temperature and σ_r the radial confinement in in MPa. (N) gives the number of samples used for calculating the mean and Δ gives the difference between the maximum and minimum value.

	T_i	$\sigma_r = 0.007$ (N)	Δ	$\sigma_r = 0.020$ (N)	Δ	$\sigma_r = 0.099$ (N)	Δ
Saline samples	-2.5°	0.177 (6)	0.306	0.186 (6)	0.399	0.126 (4)	0.122
	-8.5°	0.299 (6)	0.584	0.260 (6)	0.488	0.381 (6)	0.564
Fresh samples	-2.5°	0.045 (2)	0.037	0.218 (2)	0.282	0.208 (2)	0.125
	-8.5°	0.120 (4)	0.156	0.092 (4)	0.104	0.160 (4)	0.114

4.3.2 Shear stress - confinement development

Peak stress - confinement development

The peak shear stress vs set radial confinement σ_r and measured peak compression stress σ_z were plotted by a Mohr-Coulomb failure criterion for each submersion time and initial temperature to analyse the freeze-bond strength development with increasing confinement. The results could be divided into five different stress-confinement developments, presented below. In general the range of peak shear stresses varied within 0.025 to 0.75 MPa.

[1] Increasing peak shear stress with increasing confinement. In figure 4.8 the Mohr-circles for three saline samples of $\Delta t = 0.5$min and T_i = -8.5°C are plotted. An approximate linear increase of peak compression stress could be seen with increasing radial confinement. This behaviour was also seen for the configurations [Saline: $\Delta t = 60$min & T_i = -2.5°C, $\Delta t = 1200$min & T_i = -2.5°C, $\Delta t = 0.5$min & T_i = -8.5°C. Fresh: $\Delta t = 1$min & T_i = -2.5°C, $\Delta t = 1$min & T_i = -8.5°C, $\Delta t = 5$min & T_i = -8.5°C,]. In total 6 out of 20 configurations had this development.

For this stress development a failure slope could easily be estimated. In figure 4.8 two failure slopes were plotted. The first, a least squares line fitted to the tangent points of two and two Mohr-circles. This suggested a failure plane in the sample different from 45°. The graph indicates a failure angle of 60-70°. The second slope was a least squares line estimated from the points of peak shear and peak compression stress for the three samples. This failure slope takes into account the correct forced failure plane of 45°. The cohesion and internal friction angle was estimated from the last mentioned failure slope.

Some of the configurations only had two samples as a basis for calculating a failure slope, an example of this is shown in figure 4.9 of the fresh configuration; $\Delta t = 1$min & T_i = -8.5°C.
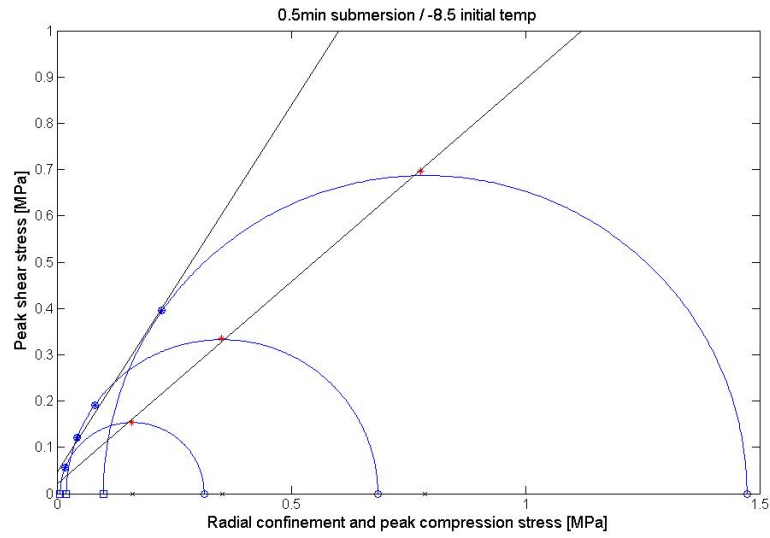
Figure 4.8: Peak shear stress σ_{FB} vs set radial confinement σ_r and measured compression stress σ_z for T_i = -8.5°C and Δt = 0.5min, saline samples.
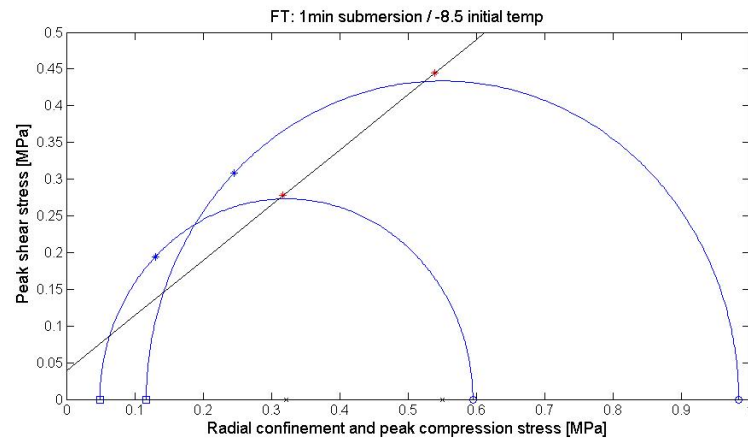
Figure 4.9: Peak shear stress σ_{FB} vs set radial confinement σ_r and measured compression stress σ_z for T_i = -8.5°C and Δt = 1min, fresh samples.

[2] **Increasing peak shear stress with increasing confinement up to 0.020MPa** This development was presented in figure 4.10 a), where the peak compression and peak shear stress increased with increasing radial confinement up to 0.020 MPa, for the highest confinement 0.099 MPa the

peak stress had a lower value than for the two previous. This development was seen for the configurations; [Saline: Δt = 1min & T_i = -2.5°C, Δt = 1min & T_i = -8.5°C. Fresh: Δt = 0.5min & T_i = -2.5°C]. In total 3 (+1) of 20 configurations. The +1 configuration refers to figure B.1c where only two samples were tested, and this could fall in to several development types, but was not used for calculations of a failure slope.

Three possible interpretations were considered, all classified as a premature failure. The first was presented in figure 4.10 b) the same graph as in a) was plotted with modified peak stress - confinement values for the sample with a confinement of 0.099 MPa. Here as a uni-axial sample, starting with no confinement and compression ($\sigma = 0$) and rising up to 0.099 MPa as maximum compression. This Mohr-circle was then in the range of the failure envelope estimated from the two other samples. This indicates that a failure may have occurred before vertical compression was applied.
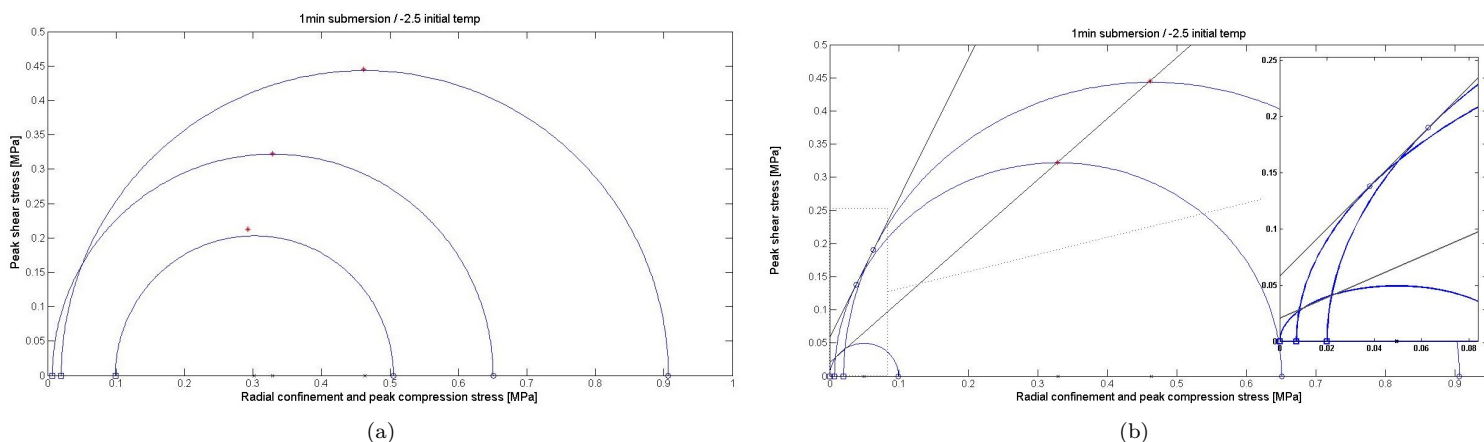
Figure 4.10: a) σ_r and measured compression stress σ_z for T_i = -2.5°C and Δt = 1min b) σ_r and measured compression stress σ_z for T_i = -2.5°C and Δt = 1min where the Mohr-circle for the highest confinement is plotted as [0, 0.099MPa]. Saline samples.

It could also be a weakness in the freeze-bond causing it to fail prematurely. And the third interpretation, that there had been softening of the material, presented below.

For both type [2] and [4] developments, two failure slopes were estimated. For type [2], the first by fitting a line through the failure points of the samples with the two lowest confinements and further extrapolating this to a second failure slope through the sample with the highest confinement. This was done by assuming the first line to give an approximately correct tensile stress and using this as a starting point for the second failure slope. For type [4] developments the same approach was used, but the two samples with highest confinement were used to estimate the failure slope. In figure 4.11 this method is shown for the configuration T_i = -2.5°C and Δt = 1min, for saline samples and development type [2]. The first failure slope was displayed as a black line, while the extrapolated one was shown as a grey line.

Only three configurations were interpreted as type [2] and six as type [4]. For type [2] the maximum difference in cohesion was 0.0054 MPa, which was in the order of 26.6% lower than the black failure slope and the minimum of 10% lower. For all the failure slopes the internal friction parameter were also in the same order less as for the cohesion.

Figure 4.11: Peak shear stress σ_{FB} vs set radial confinement σ_r and measured compression stress σ_z for T_i = -2.5°C and Δt = 1min, saline samples.

The same result revealed it self for all three configurations, the third sample with the highest confinement lay above the estimated failure slope when plotted as an uni-axial sample. Indicating failure from the confinement pressure and not the measured compressive force. The calculated values for softening was presented as a part of the discussion (5.2.3.

[3] Intermediate stress for the lowest confinement, lowest stress for the intermediate confinement and highest stress for the highest confinement. This development was seen for 2 configurations. One saline sample configuration T_i = -2.5°C & Δt = 20min and one fresh sample configuration, T_i = -8.5°C & Δt = 60min, presented in figure 4.12. In this figure a line was drawn both through the peak shear - compression stress values for the samples with lowest and highest confinement. The stress at which the sample with intermediate confinement fails, lays well below the failure envelope. This points to a prematurely failure of this particular sample, e.g. a weakness in the ice.
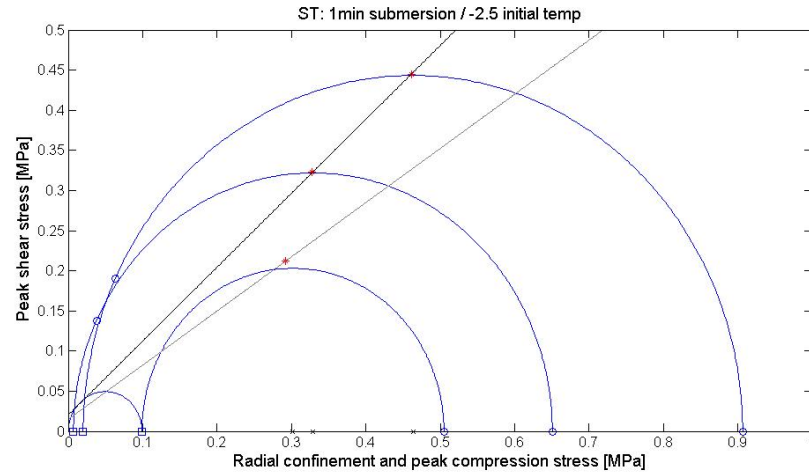
Figure 4.12: Peak shear stress σ_{FB} vs set radial confinement σ_r and measured compression stress σ_z for T_i = -8.5°C and Δt = 60min, fresh water samples.

[4] Highest peak stress for lowest confinement, lowest stress for intermediate confinement and intermediate stress for highest confinement. This development of the peak shear stress dependent of confinement was presented in figure 4.13. The highest stress was measured for the lowest confinement, the lowest stress for the intermediate confinement and the intermediate stress for the highest confinement. This suggested that the stress first increased and failed before it increased again with increasing confinement. This was seen for the configurations [Saline: Δt = 5min & T_i = -8.5°C, Δt = 20min & T_i = -8.5°C, Δt = 60min & T_i = -8.5°C, Δt = 1200min & T_i = -8.5°C. Fresh: Δt = 20min & T_i = -8.5°C, Δt = 1200min & T_i = -8.5°C]. In total 6 of 20 configurations.

The failure slope was here based on the two samples with the highest confinements. Assuming this can represent softening of the material, this was again used to draw a failure slope through the sample with lowest confinement. The opposite method as presented for type [2]. For type [4] the maximum and minimum difference in cohesion was in the same order as for type [2], 10-30% difference, also the internal friction parameter was in the same order.

For one configuration the cohesion and internal friction angle was well out of two standard deviations range. For this configuration a uni-axial sample was also tested and used to estimate another failure slope. In figure 4.14 a) the first approach was presented, giving an unusually high cohesion value and low internal friction. In figure 4.14 b) the uni-axial sample was used for the failure slope estimation, this gave a much more reasonable result, well within the range of cohesion values. This value was also used for calculating the mean cohesion value in table 4.4.
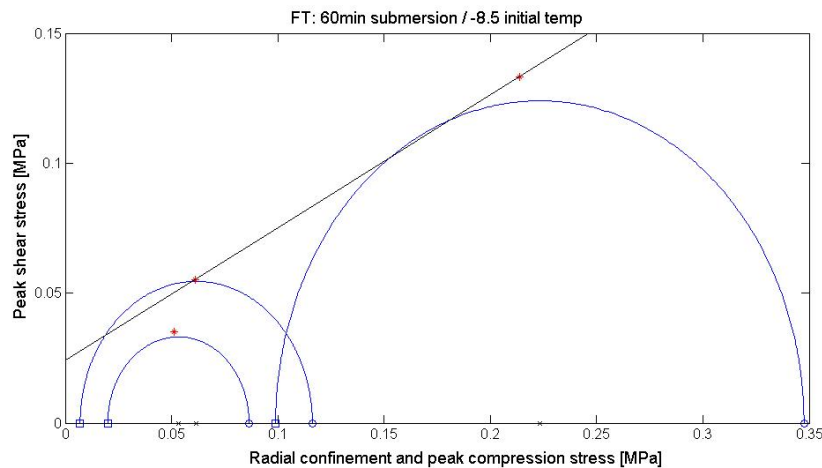
Figure 4.13: Peak shear stress σ_{FB} vs set radial confinement σ_r and measured compression stress σ_z for T_i = -8.5°C and Δt = 60min, saline samples.
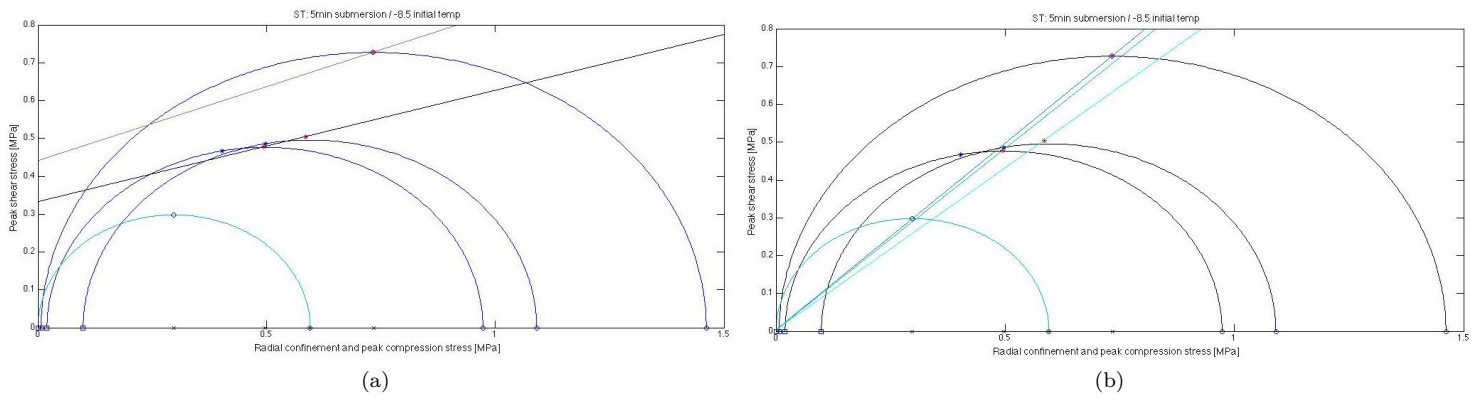
Figure 4.14: Failure slope and cohesion/internal friction values estimation for a type [4] development. a) Failure slope estimated from the two samples with highest confinement (black). b) Failure slope estimated from uni-axial sample and sample with lowest confinement (dark blue).

[5] **Decreasing stress with increasing confinement.** This development was seen for two test configurations (+1), one of them presented in figure 4.15 for T_i = -2.5°C and Δt = 5min, the other for T_i = -2.5°C and Δt = 0.5min. This development was only seen for saline experiments. For this development type no estimation of cohesion and internal friction angle could be made.
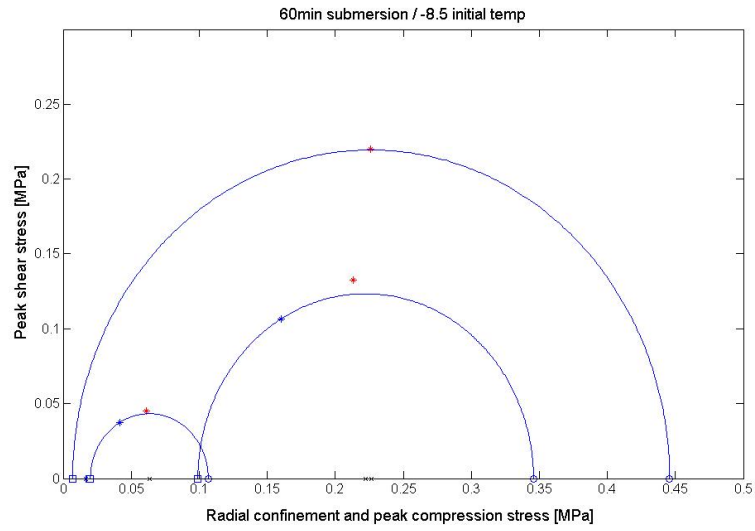

Figure 4.15: Peak shear stress σ_{FB} vs set radial confinement σ_r and measured compression stress σ_z for T_i = -2.5°C and Δt = 5min, saline samples.

**Residual stress - confinement development**

The residual stress was plotted against the set radial confinement and the residual compression stress, as for the peak stress. A generally lower stress than for the peak was observed for all samples, in a range between 0.017 - 0.08 MPa for the saline samples and 0.008 - 0.22 MPa for fresh water samples.

Studying all plots in appendix C a decrease in stress can be seen for increasing submersion times for the fresh water experiments, while for the saline samples no apparent connection could be made. The strength dependency on submersion is presented in chapter 4.3.4.

Comparing the residual stress - to the peak stress - confinement development it was seen that the development type could more often be defined as type [1], increasing stress with increasing confinement. 6 of 8 fresh water and 8 of 12 saline water configurations had this development.

The failure slopes were estimated in the same manner as for the peak stress - confinement development. In figure 4.16 the residual shear stress $\sigma_{FB,res}$ vs set radial confinement σ_r and measured residual compression stress σ_z for T_i = -8.5°C and Δt = 60min is presented with an estimated failure slope. This was a representative configuration of type [1] for the residual stresses.

In figure 4.12 the same configuration was shown for peak shear stress $\sigma_{FB,peak}$. A different development type could be seen for the peak stress. As for several of the residual shear stress - confinement developments it was more often a linear development, independent of the development type found for the peak shear stress.

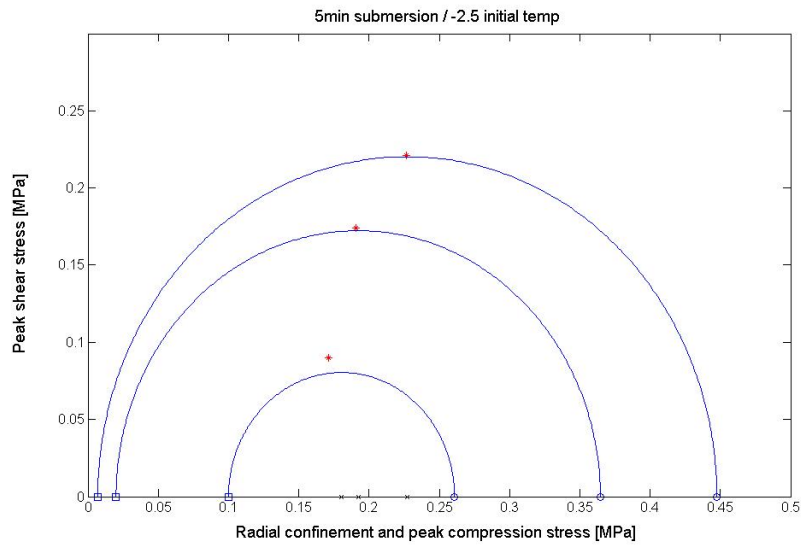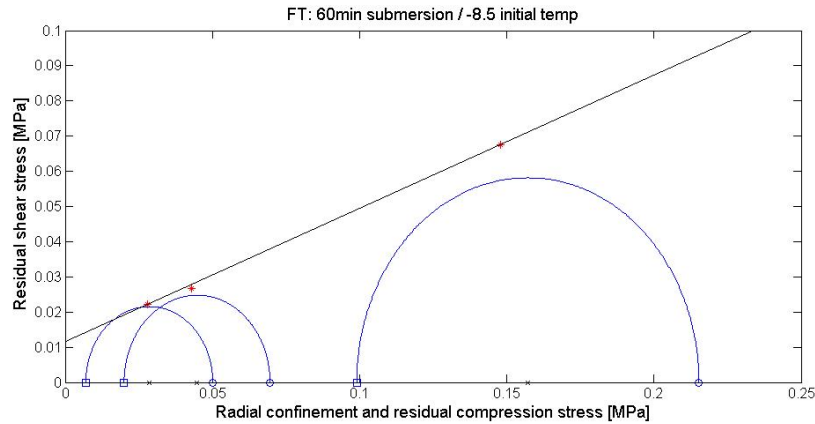Figure 4.16: Residual shear stress σ_{FB} vs set radial confinement σ_r and measured residual compression stress σ_z for T_i = -8.5°C and Δt = 60min, fresh water samples.

The developments not included in type [1] was not used for estimating failure slopes. These plots are presented in appendix C. Including the configurations with too few samples to conclude upon.

4.3.3 Cohesion and internal friction angles

The cohesions and internal friction angles has been calculated from the estimated failure slopes of the applicable peak shear stress - confinement developments. The mean values are presented in table 4.4 together with the standard deviation. The configurations with cohesion and internal friction laying well above or below two times the standard deviation was excluded, also the configurations giving negative cohesion values were not used.

Table 4.4: Mean cohesion and friction angles for peak stress

	n	Mean cohesion (c)	SD c_{SD}	Mean friction angle (ϕ)	SD (ϕ_{SD})
Fresh configurations (all)	5	0.036	$\pm0,017$	30.93°	$\pm5.69°$
-2.5°C	1	0.028	±0	27.53°	$\pm0°$
-8.5°C	4	0.038	±0.019	31.74°	$\pm5.85°$
Saline configurations	8	0.028	±0.031	35.85°	$\pm15.32°$
-2.5°C	3	0.026	±0.021	33.90°	$\pm15.31°$
-8.5°C	5	0.028	±0.036	37.25°	$\pm14.69°$

In total 5 fresh water configurations and 8 saline configurations were used for the calculations. The range of cohesion for all configurations were 0.003-0.099MPa. The mean cohesion was lower at the initial temperature of -2.5 than -8.5°C for both the fresh water and saline samples. The cohesion was approximately 30% higher for the fresh configurations than the saline. The standard deviation of the fresh configuration represent a lower spread than for the saline configurations, which could also be a result of fewer total configurations as a sample basis.

The internal friction angles were in the range 16.21 to 44.70° for all configurations. The mean friction angles were higher for saline configurations than fresh and also for the lowest initial temperature. The variability was also higher for the saline configurations, which could be seen by the standard deviation of 15.32° compared to 5.69° for the fresh configurations. Also here the same sample basis may have had an effect.

A failure slopes was also estimated for the residual stress - confinement developments, the mean cohesions and internal friction angles are presented in table 4.5.

Table 4.5: Mean cohesion and friction angles for residual stress

	n	Mean cohesion (c)	SD c_{SD}	Mean friction angle (ϕ)	SD (ϕ_{SD})
Fresh configurations (all)	5	0.007	$\pm0,003$	23.47°	$\pm10.54°$
-2.5°C	1	0.006	±0.002	23.18°	$\pm8.10°$
-8.5°C	4	0.008	±0.006	23.62°	$\pm3.05°$
Saline configurations	7	0.009	±0.006	25.03°	$\pm10.00°$
-2.5°C	3	0.006	±0.003	25.86°	$\pm11.81°$
-8.5°C	4	0.011	±0.006	24.40°	$\pm7.85°$

The mean cohesions found for the residual stress were lower than for the peak stress, also the internal friction angles were found to be lower. The range of cohesions vary from 0.0010 to 0.0179 MPa. The same trend of higher values of cohesion for the lower initial temperature can be seen here for both saline and fresh configurations. No apparent difference between the fresh and saline configurations can be made from these results.

The range of internal friction vary from 11.21 to 36.70°. This was within the range of what was found for the peak stress, but in the lower part. This could also be said for the mean internal friction. The standard deviations were lower, indicating more stable results, which also would be expected.

The mean friction angles were calculated to be higher for all the saline configurations than for the fresh. No connection could be made towards the initial temperature.

4.3.4 Submersion time Δt

In figure 4.17 the freeze-bond shear stress τ_{FB} is plotted according to submersion time Δt, the saline water experiments in figure 4.17 a) and the fresh water in b). The freeze-bond strength was tested for six submersion times. A bell-curve trend can be seen for both saline and fresh samples. An increase in strength up to 5 min submersion time and then a following decrease was found.

For the samples with initial temperature T_i of -8.5°C the highest confinement in general gave the highest shear stress. The peak strength was seen after 0.5 min for the saline experiments and after 1 min for the fresh water experiments.
For the saline experiments the peak shear stress was seen at 5 min and 1 min for the confinement 0.007 MPa and 0.020 MPa accordingly. For the highest confinement a peak was seen at 0.5 min.
For the two lower confinement values for the fresh water samples,the freeze-bond shear stress deviated from the "perfect" bell-curve. For both the intermediate and lowest value the strength-curve had a secondary peak in addition to the first, at 1 min and 20 min for 0.007 MPa and 0.5 min and 20 min for 0.0020 MPa. For the highest confinement a peak was seen at 1 min.

For the saline experiments with initial temperature T_i of -2.5°C the stress development deviated from the bell-curve with secondary peaks for confinements 0.020 MPa and 0.099 MPa, with peaks at 1min/60 min and 1min/20 min accordingly. For the lowest confinement the strength developed as a bell-curve with a peak at 0.5 min or earlier.
Because of very low freeze-bond strength for longer submersions than 1 min, no fresh samples were tested with initial temperature of -2.5°C for longer submersion times. For confinement 0.020 MPa and 0.099 MPa a peak was seen for 0.5 min, for the lowest confinement the peak stress was located at a submersion time of 1 min or higher.
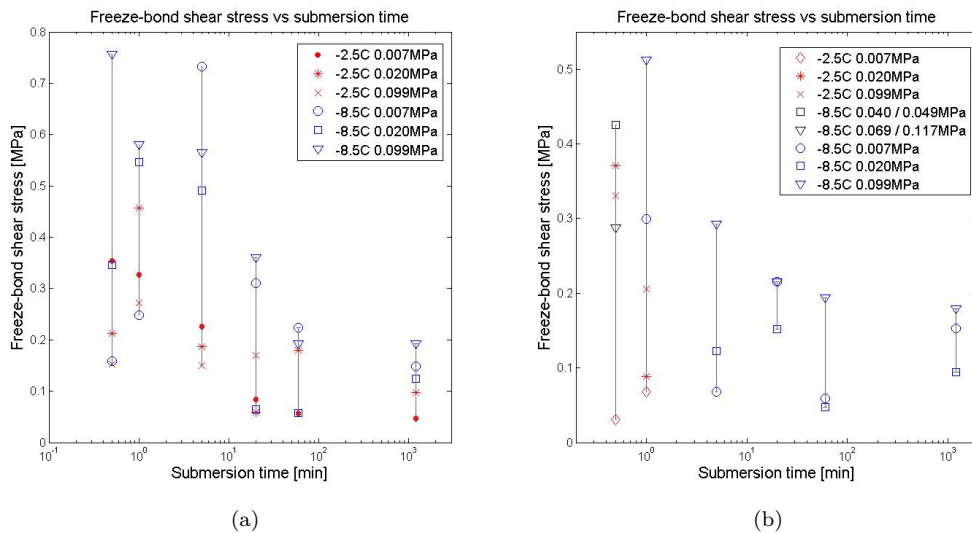
Figure 4.17: Submersion time Δt vs freeze-bond shear stress τ_{FB}. a) saline water experiments b) for all fresh water experiments

While testing the samples it was observed that the fresh water samples decreased in size during submersion. The highest decrease was seen for samples with initial temperature of -2.5°C. The saline samples increased in size during submersion, this was especially evident for the longest submersion time of 1200 min. An example of this phenomenon is seen in figure 4.18, sample ST-4 before and after submersion.

(a) (b)
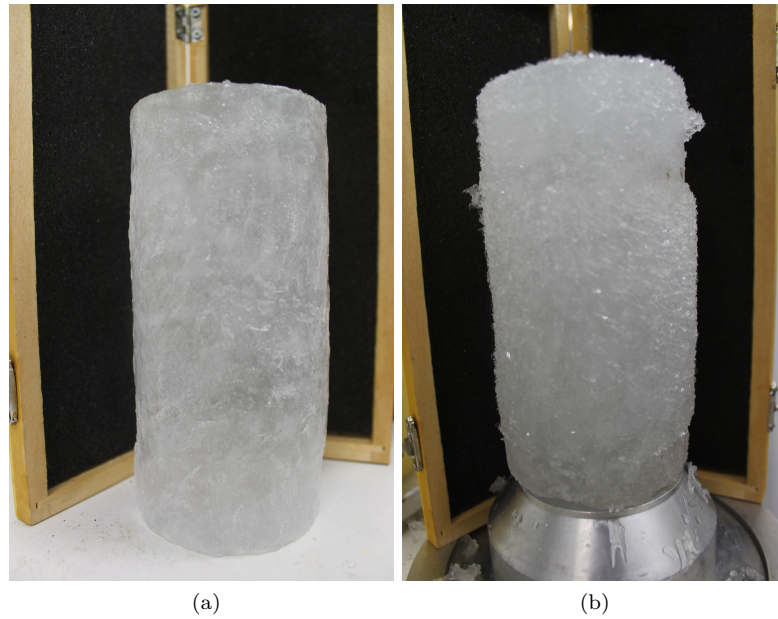
Figure 4.18: Sample ST-4 Δt = 20min T_i = -2.5°C a) before submersion b) after submersion

4.3.5 Initial temperature T_i

In figure 4.19 the peak freeze-bond shear stress $\tau_{FB,max}$ was plotted against the initial temperature of the ice both for the saline samples and the fresh samples. For both, the maximum shear stress was higher for -8.5°C than for -2.5°C. The highest measured shear stress was also higher for the fresh ice at both temperatures. The lowest measured stress was on the other hand in the same range for both the temperature and the salinity, this means a large range of shear stresses for the fresh samples and at the initial temperature of -8.5°C.

The average shear stress was plotted on the same graph according to confinement and a line was drawn between the two temperatures. For the saline samples the average strength decreased with increasing temperature. For the fresh it decreased for only the lowest confinement and increased for the intermediate and highest. There was a small sample basis of the fresh configurations with initial temperature -2.5°C.

(a)

(b)
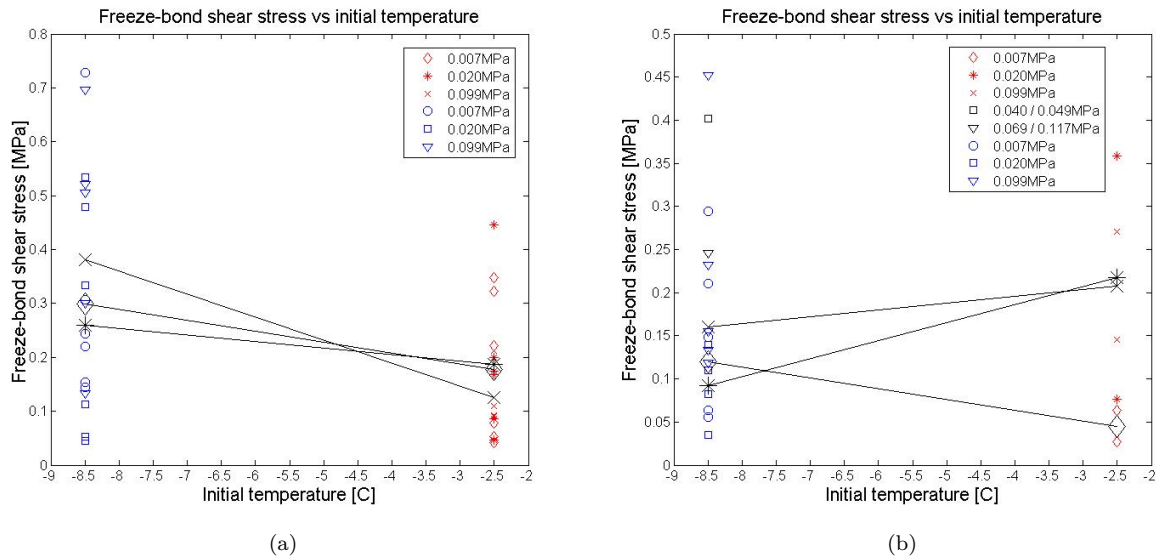
Figure 4.19: Initial temperature vs peak freeze-bond shear stress. Lines between average value of each confinement. a) saline water samples b) fresh water samples

After the compression test was run the temperature was measured both near the freeze-bond and at the top of the sample. In figure 4.20 all samples were plotted for the temperature measured before and after testing. A relation between submersion time and temperature can be made out, for longer submersion times the ice approaches the temperature of the water. Both for the initial temperature of -2.5°C and -8.5°C, the sample temperature was in equilibrium with the water at 1200 min, which means that this occurred between 60 and 1200 min. In figure 4.20 a) the samples with submersion times 0.5 and 1 min seemed to hold about the same temperature as the initial -2.5°C, this was not seen in figure b) for initial temperature of -8.5°C, where the temperature changed at even the

shortest submersion times. Because of the higher temperature gradient the mobilization time for temperature change could be lower.

No apparent connection could be made between the measured temperature after testing by the freeze-bonded section and the top of the sample.

Sample ST-7 and ST-8 had a measured temperature after testing which was lower than the initial, this was likely a measurement error, maybe due to the cooling fans in the Cold Lab.

(a)   (b)
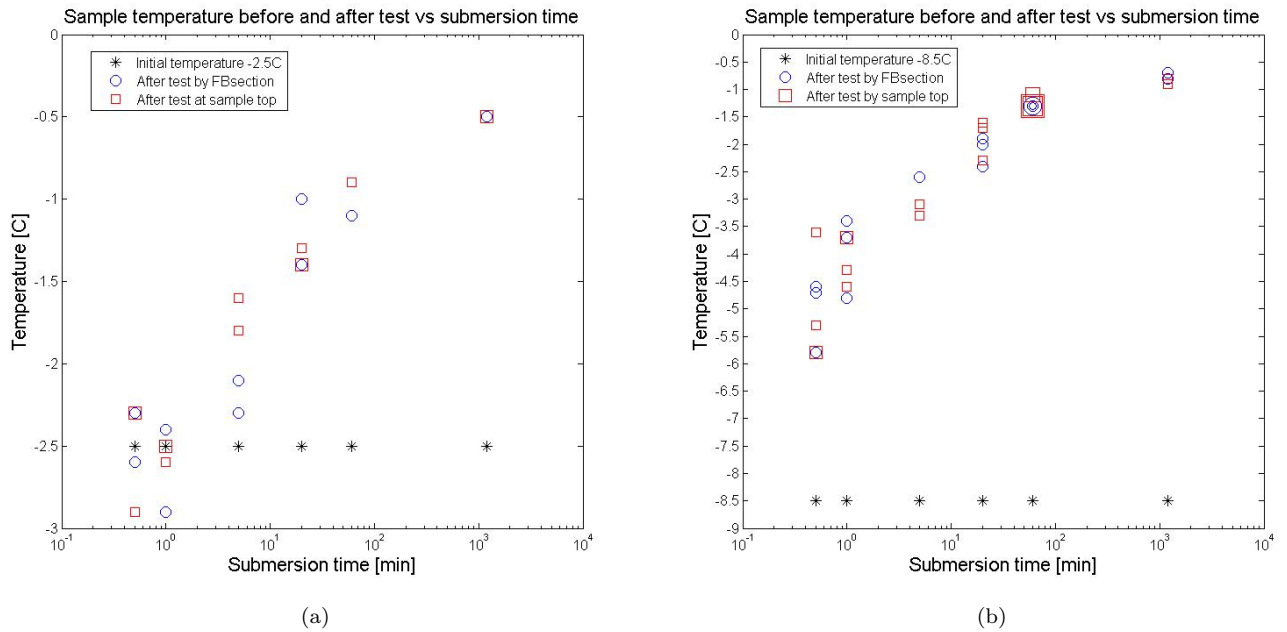
Figure 4.20: Initial temperature, temperature by the freeze-bonded section and at the sample end after testing a) initial temperature Δt = -2.5°C b) initial temperature Δt = -8.5°C

4.3.6 Salinity development

The salinity was measured for one or a few samples before testing, and for each sample after testing. In table 4.6 the salinity before testing (S) and the average salinity of all samples after testing $(S_{i,avr})$ are shown for each ice sheet. The average salinity increased for the fresh water samples to approximately the salinity of the submersion water. For the saline samples the average salinity decreased after testing, suggesting drainage of brine during submersion. Only two samples were used for tri-axial testing from Sheet 3, which gave a small sample basis. The salinity was measured to remain the same before and after testing for this sheet.

Table 4.6: Salinity before (S) and average salinity of all samples after testing $(S_{i,avr})$

	S [ppt]	$S_{i,avr}$ [ppt]
Fresh water samples	0.003	0.056
Sheet 1	2.25	2.01
Sheet 2	2.27	2.09
Sheet 3	2.76	2.76

In figure 4.21 a) the salinity measurements after testing are displayed for all saline samples. They are displayed two and two together where the only configurational difference was initial temperature displayed in red for -2.5°C and blue for -8.5°C. In 11 of 16 configurations the highest initial temperature, -2.5°C, had the lowest salinity. Due to longer drainage times the salinity was generally lower for longer submersion times, but there was also seen relatively large variations.

In figure 4.21 b) all salinities are displayed depending on submersion time. Here it was clear that the salinity after 0.5 and 1 min remained as before submersion and that it had decreased for the two longest submersion times. For the intermediate submersion times, 5 and 20 min, the salinity had a larger variation between each sample.

(a)

(b)
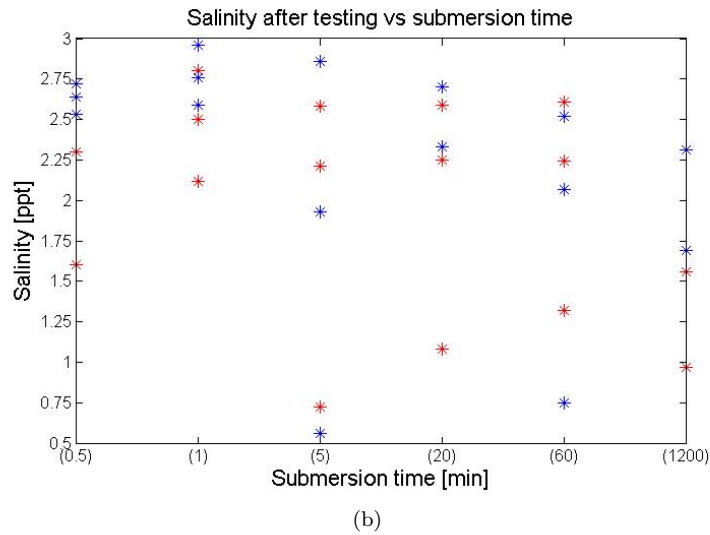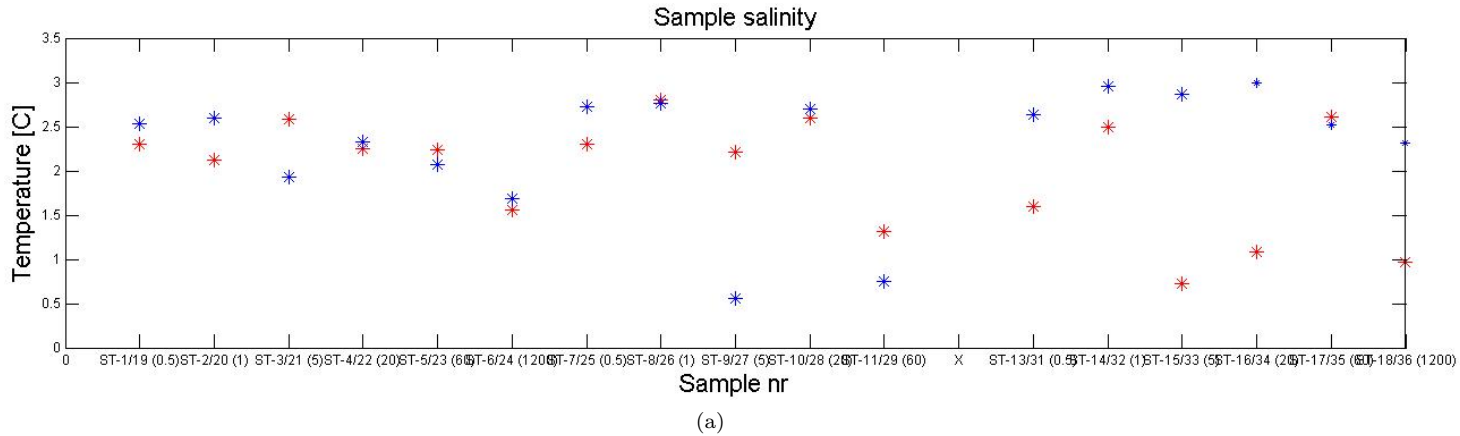
Figure 4.21: a) Salinity for all saline samples after testing. Red dots for samples of initial temperature of -2.5°C of -8.5°C. b) Salinity for all saline samples after testing vs submersion time.

Comparing the fresh and saline experiments the peak strength range was higher for the saline samples while the residual strength was higher for the fresh samples. The peak shear stresses for saline samples were in the range of 0.04 to 0.70 MPa. For the fresh samples from 0.025 to 0.44 MPa. And for the residual stresses 0.017 to 0.08 MPa for the saline and 0.008 - 0.22 MPa for the fresh.

Chapter 5

Discussion

A discussion of the results are presented in this chapter. It is presented in the same order as the result chapter. The fracture behaviour observed in the experiments are discussed together with the plotted failure modes. The next section will address the parameters influencing the freeze-bond stress, with main focus on the stress - confinement development. The results will here also be compared with previous studies on the effect of confinement on freeze-bond stress.

In the last section the experimental procedure will be discussed and the flaws and strengths remarked.

5.1   Failure modes

The samples was defined as either failing brittle-like or ductile-like in chapter 4.2, in addition the observed fracture behaviour during testing was presented in sub-chapters 4.2.1 and 4.2.2.

Both brittle and ductile behaviour was found to occur. All samples defined as ductile failed by freeze-bond sliding and was found to have a comparatively lower strength. Repetto-Llamazares et al. [2011a] also concluded that the samples failing ductile-like had a lower strength. It was argued that a higher strength may lead to a steeper unloading slope due to more elastic energy being released.

The ductile failure mode was observed at longer submersion times, usually from 20 min or longer, only with a few exceptions. The number of ductile failures was larger for the higher initial temperature of -2.5°C. Samples with a higher initial temperature has less potential energy and thus less energy to form freeze-bonds. It is proposed by Repetto-Llamazares et al. [2011a] that the strength development under submersion is a development of the porosity (see chapter 2.3.1). At longer submersion times, when the brine drains and the temperature rises again, the porosity increases and the freeze-bond strength decreases.

Applying the brittle - ductile transition theory of Schulson et al. [2009] and that a reason for a lower strength could be higher porosity, this will shift the transition point and a sample may have a ductile behaviour for a set compression rate. And as explained above the ductile-like samples are already in the lower range of strengths, and as the results point out, probably close to the transition

51

point. This makes them susceptible to small changes like ruff handling or less precision when fixing the samples for submersion.

The brittle failure mode includes two types of shear stress - run time plots. The first where it increased to a peak load, failed and stabilized on a constant load. This was the most common. The other where the load increased to a maximum, failed and built up again to a new peak, creating a series of failure points. While testing this could be heard as a continues cracking sound from the sample. It was most often seen for samples with the lowest initial temperature, at short to intermediate submersion times and only for fresh water samples. These samples may still have potential energy, they have not reached equilibrium, to form freeze-bonds when they are tested. The freeze-bond first breaks and slides and before the piston load has built up the force, a new freeze-bond has formed. This will explain the continues breaking sound, which was distinct for these samples.

The observed fracture behaviour during testing varied between three types, sliding along the freeze-bond, splitting and crushing. Only samples of the first type or a combination of the first and second was used for calculations. The two last types was determined as ice failure. Splitting occurred only for short submersion times, when the freeze-bond is at it's strongest. This means that any weakness in the sample may cause it to fail prior to the freeze-bond. A weakness may be induced by ruff handling during drilling and preparations or during ice production, e.g a brine pocket. Idealized the piston will distribute the force evenly over the sample, but after submersion the surface may not be completely level. This can also induce failure in the ice, by only applying load to a small part of the sample. This was seen by that one edge was either split or crushed, often in combination with sliding along the freeze-bond. One question that then arises is if the load is evenly distributed over the freeze-bond section or if it is affected by the previously weakened part. But the strength of the few samples where this occurred does not deviate from the norm.

Each fracture behaviour had a specific force - run time plot which confirmed the observed behaviour, but the difference between crushing of the whole sample or crushing of just an edge combined with sliding was hard to differentiate. A subtle difference between sliding and the combined splitting and sliding could be observed on the loading slope.

No obvious connection between the failure mode and the radial confinement could be made.

From table 4.1 it was evident that the fresh samples had a larger effect of the temperature difference than the saline.

To sum up. The brittle samples were observed to have higher strengths. The ductile behaviour only occurred for the weakest samples, i.e. long submersion times and high initial temperatures. Also two fracture types was observed for the brittle-like samples, which was used for further calculations. Sliding over the freeze-bonds and a combination of sliding and splitting. Where for the last the sample first fails locally by splitting, then fails by sliding.

5.2 Freeze-bond strength

The experimental set-up for testing the freeze-bond strength was the same as for Møllegaard [2012] for the uni-axial samples. In general the freeze-bond strength was found to be in the same order, but in the lower range, which could be a result of shorter samples. This comparison was done in order to ensure comparable results even though radially confined tests have not been conducted with this set-up previously.

To analyse the results and deduce what mechanical processes involved, Mohr-Coulomb plots were constructed for the different configurations. A linear failure slope was chosen because of few data point for each configuration, which may not have given an appropriate representation. A line drawn thorough the peak shear stress points gave the best fit, and included the forced failure plane of 45°. To envelope the entire circles a slope suggesting a failure plane of 60-70° in the sample was the best fit. The first failure slope was used for calculating the cohesion and internal friction angles. Why a failure slope, indicating a steeper failure plane, was fitting for enveloping was unknown.

5.2.1 Confinement σ

The peak shear stress $\tau_{FB,peak}$ was plotted against the peak normal stress $\sigma_{FB,peak}$ for all samples. They were separated between initial temperature T_i and confinement σ_r. The mean value of $\tau_{FB,peak}$ was also calculated for the same variables.

The highest internal stresses were seen for all confinements at the lowest initial temperature, -8.5°C, for the saline samples. This tells us that the temperature difference had a higher effect than the confinement in this range.

For the fresh samples the internal stresses were only higher for the lowest confinement at -8.5°C. A reason for this could be that only samples for the two shortest submersion times were tested for fresh samples at -2.5°C and only the 4 longest submersion times were used for -2.5°C. According to theory samples of shorter submersion times should be stronger than for equivalent samples at longer submersion times. And this may have a stronger effect than the temperature difference in this case.

For both saline and fresh samples there was a general increase in internal stresses with increasing confinement. Defined by, the peak stress always being higher for the highest confinement than for the lowest. In more detail, for the initial temperature of -2.5°C the intermediate confinement had the highest mean stress. For -8.5°C the intermediate confinement had the lowest mean stress. The reason for these variations was unclear.

5.2.2 Shear stress - confinement development

The shear stress was plotted against the radial confinement and the compression stress in a Mohr-Coulomb plot. It could be differentiated between five different developments listed below. Each will be discussed in relation to how it describes the material and the physical mechanism it may have derived from.

- [1] Increasing shear stress with increasing confinement

- [2] Increasing peak shear stress with increasing confinement up to 0.020MPa

- [3] Intermediated stress can be seen for the lowest confinement, lowest stress for the intermediate confinement and highest stress for the highest confinement

- [4] Highest peak stress for lowest confinement, lowest stress for intermediate confinement and intermediate stress for highest confinement

- [5] Decreasing stress with increasing confinement

[**1**]. This type of development is what has been found in previous studies using the classical experimental approach as presented in chapter 2.2. 6 out of 20 peak shear stress configurations and 14 of 20 residual shear stress configurations had this development. This suggests a Mohr-Coulomb like failure mode to be appropriate.

The failure slope covering the whole mohr-circle suggested a failure angle of 60-70°, as for coulombic shear faulting (defined in [Schulson et al., 2009]). In reality this was forced to 45° during testing. The sample was assumed to consist of one element, which implies that it is homogeneous. A possibility for the differentiating angles could be local faulting at 60-70° along the freeze-bond.
[**2**]. A linear increase with confinement was also seen for this development type up to 0.020 MPa. Of the peak shear stress configurations 3 (+1) configurations were defined as type [2]. The +1 could fit for several development types because it only had two samples. For the residual shear stress there was 2 (+1) configurations, 1 uncertain due to few samples. One of the residual configurations could also have been defined as type [1]. It was chosen to be presented as type [2] because the cohesion was abnormally large and the internal friction angle was too small when the failure slope was estimated as type [1].

There was three possible interpretations of this development. The first, a weakness in the sample caused it to fail prematurely (can arise from how it was treated during experiments or when it was made). The second, that there was a softening of the material. And the last that the radial confinement exceeded the strength of the freeze-bond and that it had already failed before the vertical compression was applied.

The third interpretation was tested by plotting the "failed" sample as uni-axial with the peak compression force equal to the set radial confinement. It was then possible to see if it crossed the estimated failure slope of the two other samples and failing before the test started. This seemed appropriate for all configurations and these failure slopes were used for estimating cohesion and internal friction values. For one residual configuration, both the second and third interpretation could fit, softening or failure of the sample before vertical compression. The interpretation of softening was investigated as explained in chapter 4.3.2. For this approach the first estimated slope was assumed to give a correct tensile stress. If this assumption was suitable is unknown.

[**3**]. 2 peak shear stress configurations and 4 residual shear stress configurations of in total 40 configurations. An explanation to this development was that the sample of intermediate stress failed prematurely. A failure slope was estimated based on the two other samples and the cohesion and internal friction angle was in range of the values from type [1].

[**4**]. This development occurred for 6 of 20 peak configurations and no residual configurations. This development suggested that the stress increased and failed before it again increased for increasing confinement. The explanation for this was likely to be coincidence. E.i. some of the samples failed prematurely due to e.g. weaknesses in the ice or freeze-bond. Another explanation could have been that there was a threshold where the confinement starts to have an effect of the freeze-bond strength. Very few configurations had this type of development and this points towards coincidence.

Some of the configurations were used for calculating a failure slope with the opposite approach of type [2] for softening. The two samples with highest confinement were used to estimate a slope and then extrapolated to the sample with lowest confinement by keeping the intercept of the x-axis constant. It can be argued if it was correct to include these values in the average mean. The reason for this decision was that they were well within the range of the values from type [1].

[**5**]. Decreasing stress with increasing confinement was seen for only two saline peak configurations. This is believed to be a result of weaknesses in the samples or freeze-bonds. There is no logical physical explanation to why this occurred other than coincidence.

Peak stress - confinement development

In total five different developments for the peak stress dependency on confinement was found. The first type was what was expected to be found, a linear increasing stress with increasing confinement. Also the second and third type could be argued that it represents the same type of dependency, but because of the high degree of uncertainties when testing ice, some modification and interpretation was needed. If the first three types were assumed to represent increasing stress with increasing confinement, in total 11 (+1) of 20 configurations had this development.

The type [4] development consists of 4 saline configurations, with submersion times of 5, 20, 60 and 1200 min, and 2 fresh configurations with submersion times of 20 and 1200 min. All with the initial temperature of -8.5°C. The samples of longer submersion times were considered to be weaker, but the lower initial temperature should increase the strength. The lowest confinement gave the highest measured stresses for this type, a reason for this could be that the freeze-bond strength was too low and failed when the radial confinement was applied. The fifth development type consisted of two configurations, both saline for 0.5 and 5 min submersion times and -2.5°C. The configurations with short submersion times and low initial temperature was observed to be easily affected by small changes in how the experiment was conducted, this was seen by large variations in strength during testing.

The first two development types were represented by the shortest submersion times of 0.5, 1 and 5 min. Type [3] was represented by two configurations, one fresh T_i = -8.5°C & Δt = 60 min and one saline T_i = -2.5°C & Δt = 20 min. These are the only two samples considered to represent linear increasing stress with increasing confinement with longer submersion times. As suggested above the samples with longer submersion times may have been too weak for the radial confinement. If the radial and vertical force was applied simultaneously a different result may have revealed it self.

Comparing the saline and fresh configurations the saline samples had higher stresses. They were in the range of 0.04 to 0.70 MPa while for the fresh 0.025 to 0.44 MPa.

Residual stress - confinement development

The residual stress was in general lower than the peak stress for all confinements. This was as expected as the residual force is assumed to represent only the frictional force of the freeze-bond. The saline had a range of stresses between 0.017 - 0.08 MPa and the fresh a range between 0.008 - 0.22 MPa. The fresh configurations were stronger than for the saline. Lower salinity is believed to give stronger freeze-bonds. That the residual stress behaves in the same manner suggests that also the friction is affected. Continuously forming of freeze-bonds during compression was suggested in chapter 4.2, if this is the case, this could also give rise to the higher measured stresses.

Compared to the peak stress - confinement development the residual stress - confinement development was more often defined as type [1]. 6 of 8 fresh configurations and 8 of 12 saline configurations was determined to have increasing stress with increasing confinement. This can be explained by that the frictional force is less susceptible to small experimental differences than the freeze-bond.

The configurations that did not fit type [1] development consisted of 2 fresh (0.5 and 20 min submersion times with -8.5°C) and 4 saline (0.5 and 20 min with -2.5°C and 5 and 20 min with -8.5°C).

5.2.3 Cohesion and internal friction angles

The cohesion and internal friction angles were calculated from the estimated failure slopes described previously, both for peak and residual shear stresses. Comparing these, the mean cohesion values were found to be lower for the residual stress and the internal friction values lies in the lower part of the range of the peak stresses. The standard deviations were also found to be smaller for the residual stresses, indicating more stable results. This would be expected from the assumption that the residual stress represents friction which is less dependent on the small deviations between tests and between each sample.

Comparing the fresh and saline configurations the mean cohesion values were found to be 30% higher for the fresh than saline for the peak shear stresses. For the residual the cohesion values were all close to zero as expected, but the saline were higher. The mean internal friction angles were higher for the saline configurations for both the peak and residual stresses. Indicating that the stress of the fresh samples were less influenced by increasing confinement.

A temperature dependency was also visible from the results. All mean cohesion values were higher for the lower initial temperature of -8.5°C. As explained in chapter 2.3.3 the freeze-bond has been found to have increasing strength for decreasing temperatures, which also would account for this finding.

The cohesion values were in the range of 0.003 - 0.099 MPa and the internal friction 16.21 - 44.70° for the peak stresses. For the residual 0.001 - 0.018 MPa and 11.21 - 36.70°. Repetto-Llamazares et al. [2011a] found cohesion values in the range of 0.0011-0.0044 MPa and internal friction values in the range 11-34°. And Serré [2011] found the cohesion to be 0 and the internal friction as 30-45°. Quite similar results even though two different test set-ups were used.

For type [2] and [4] two failure slopes were considered. One representing softening of the material.

For all configurations the cohesion values and internal friction angles for the slope representing softening were in an order of 10-30% lower. This was not studied further because the larger part of the samples was interpreted as failing before testing, when the radial confinement was applied.

The negative cohesion values were not used for calculating the mean. This may not give the best representation and may have given higher cohesion values.

5.2.4 Submersion time Δt

The freeze-bond stress was plotted against the submersion time. In general a bell-curve development of the stress could be seen, as found in previous studies. The sample were not confined when submerged, so that the same development as previously found was expected.

For the initial temperature -8.5°C all peak stresses were seen for 5 min or shorter submersion times. For all confinements the peak stress was reached at 1 min for the saline samples and 0.5 min for the fresh. With the initial temperature of -2.5°C all peak stresses were seen for 1 min or shorter submersion times. For all confinements the peak stress was reached at 1 min for the saline samples and 0.5 min for the fresh. There was a very small sample basis for the fresh samples, only tests for 0.5 min and 1 min submersion times were conducted.

The fresh water samples generally peaked at shorter submersion times. A lower porosity in these samples increases the thermal conductivity. Air filled pockets also has a higher mass diffusion than brine filled pockets. This suggests that the potential energy will be transferred at a higher rate for fresh ice, causing the strength to peak at an earlier time.

During the experiments it was observed that the saline samples increases in size during submersion while the fresh samples decreased.

5.2.5 Initial temperature T_i

The temperature development of the ice is closely related to the freeze-bond strength. Higher ice temperatures has less potential energy to form freeze-bonds. The shear stress was found to be higher for the lowest initial temperature, for both fresh and saline water. Shafrova and Høyland [2008] found the same trend for submerged fresh water samples, while Repetto-Llamazares et al. [2011a] only found a clear trend for the lowest confinement and this was the opposite of what was found here (increasing stress with increasing initial temperature). The lower measured stresses were found to be in the same range for both initial temperatures and for all submersion times.
The initial temperature has two effects on the freeze-bond stress. Firstly a lower initial temperature takes longer before it reaches equilibrium with the water, meaning that the sample may still be colder than the water during testing. This also affects the brine content, faster ice growth gives more brine. Secondly the speed of which the freeze-bonds are formed is higher.

The temperature development in the ice varied for the two initial temperatures. The samples at -2.5°C stayed at this temperature for the submersion times of 0.5 and 1 min, before it started to rise. The samples at -8.5°C had increasing temperatures from the shortest submersion time. The higher temperature gradient may explain the faster change. For both, the temperature reached

equilibrium with the submersion water between 60 and 1200 min.

No apparent connection could be made between the measured temperature after testing by the freeze-bonded section and by the top of the sample. The only apparent observation was that there was a difference.

Sample ST-7 and ST-8 had a measured temperature after testing lower than the initial, this was likely a measurement error.

5.2.6 Salinity development

The salinity was measured both before and after testing to study it's development. The salinity of the fresh water samples increased to that of the submersion water, which was still very low. This means that the freeze-bonds must have had a higher salinity than the surrounding ice and that not much salt was expelled, even for longer submersion times. The measured salinities were still not high enough to affect the freeze-bond strength to any degree.

For the saline samples the salinity decreased during submersion. This was assumed to result from brine drainage over time. This agrees with what was found by Møllegaard [2012], he also found that it varied in the plane, more drainage at the edges. In these experiments the freeze-bond section amounted to a relatively small area, making the drainage of brine a visible effect. For the intermediate submersion times of 5 and 20 min there were large variations in the salinity, indicating that drainage was on-going at this stage.

The lowest salinities were measured for the highest initial temperature of -2.5°C for most samples. Likely this was due to the well known fact that faster ice growth locks in more brine. A lower salinity gives higher freeze-bond strength, but at the same time the lower temperature gives a lower strength.

5.2.7 Evaluation of experimental procedure

In general the experimental test set-up was considered to be beneficial on the points that it had previously been used for uni-axial samples with the same equipment, it was relatively easy to deduce the stresses and that a pressure clock was available to use on cylindrical samples. During testing it was found to work well, with only a few disadvantages.

The pressure clock was not adapted for the 175 mm hight of the ice cores, which has been used for previous studies, the sample tested had to be no more than 150 mm. A few times the sample was impossible to remove from the clock, and it had to be melted. The pressure valve was also a point of uncertainty since it had to be manually adjusted, after a few tries this was learned. A rubber was used to spread the radial pressure evenly around the sample, when the pressure was set too high it expanded underneath the outer frame and lifted it. The radial pressure could therefore not be higher than 0.099 MPa, even at this pressure there was some trouble. And the valve restricted the lower range to 0.007 MPa. Below this point the pressure could not be kept stable throughout the test.

The temperature was measured after testing by the freeze-bonded section and by the top of the sample. More accurate measurements were needed to draw any conclusions. And the ceiling-fans in the lab have had to been switched off, also the time of testing varied due to a higher focus on conducting the compression tests.

Mohr-Coulomb plots were constructed to analyse the results. With few data points for each plot there were several ways to interpret them, resulting in uncertainties.

Chapter 6

Conclusion

The failure mode was determined for all samples. Both brittle- and ductile-like behaviour was found to occur. Samples defined as ductile-like all failed by freeze-bond sliding and was found to have a comparatively lower strength. Applying the brittle - ductile transition theory of [Schulson et al., 2009] and that higher porosity gives lower strength, the transition point will be shifted and a sample may behave ductile-like for a set compression rate normally giving brittle behaviour. The ductile-like samples were in the lower range of strengths (longer submersion times and higher initial temperatures), probably close to the transition point. This made them susceptible to small changes like ruff handling or less precision when fixing the samples for submersion.

The brittle failure mode included two types of shear stress - run time plots. The first where it increased to a peak load, failed and stabilized on a constant load. This was the most common. The other where the load increased to a maximum, failed and built up again to a new peak, creating a series of failure points. While testing this could be heard as a continues cracking sound from the sample. This only occurred for fresh samples of the strongest configurations. It was suggested that this may have been freeze-bonds continuously forming during compression.

The observed fracture behaviour during testing varied between three types, sliding along the freeze-bond, splitting and crushing. Only samples of the first type or a combination of the first and second were used for calculations. The two last types were defined as ice failure. Each fracture behaviour had a specific force - run time plot, which confirms the observed behaviour. The difference between crushing of the whole sample or crushing of just an edge combined with sliding was hard to differentiate from the plots. A subtle difference between sliding and the combined splitting and sliding could be observed on the loading slope.

No obvious connection between the failure mode and the radial confinement could be made.

The freeze-bond stresses were found to be in the same range for the uni-axial samples as found for previous experiments. It's dependency of submersion time, initial temperature and salinity was all found to reinforce the existing theory. This gave a good basis for studying the effect of radial

confinement.

The majority of the Mohr-Coulomb plots pointed towards increasing stress with increasing confinement. Due to few data points several of the plots were also defined as to be affected by weaknesses in the freeze-bond giving lower stresses than expected and therefore inconsistencies in relation to the linear increase. The cohesion found for the peak stresses were in the range 0.003 - 0.099 MPa and the internal friction angle 16.21 - 44.70°. And for residual stresses the cohesion was approaching zero and the internal friction angles were in the range 11.21 - 36.70°. Compared to previous studies these results were in the same range, even though another test set-up was used.

Comparing the fresh with the saline configurations the mean cohesion values were found to be 30% higher. The mean internal friction angles were higher for the saline configurations. A dependency on initial temperature was also seen by the cohesion values, higher cohesion for the lower initial temperature.

In general the configurations defined as having increasing stress with increasing confinement had short submersion times. This was interpreted to be a result of samples with longer submersion times may have been too weak for the applied radial confinement. It the radial and vertical force were applied simultaneously this might have given more consistent results for the weaker samples.

6.1   Further work and recommendations

The pressure clock can be modified so that samples of 175 mm can be tested. A less yielding rubber could also be used in order for it to not expand outside of the outer frame.

Supplementary tests for each configuration should be conducted in order to analyse the results in more detail.

Temperature measurements in several points along the sample after submersion may be interesting to study in order to compare with the submersion times, porosity and strength developments of the freeze-bond.

Radial confinement during submersion as well as for during compression.

Study the failure envelope of the Mohr-circles and why a steeper failure plane was suggested. What failure slope can one get by using a forced failure slope in the experiments different from 45°

Chapter 7

Bibliography

Oda Skog Astrup. Experimental investigations of ice rubble: Shear box and pile testing. 2012.

R Ettema and JA Schaefer. Experiments on freeze-bonding between ice blocks in floating ice rubble. *Journal of Glaciology*, 32(112):397–403, 1986.

Robert Ettema and Gilberto E Urroz. On internal friction and cohesion in unconsolidated ice rubble. *Cold Regions Science and Technology*, 16(3):237–247, 1989.

Henning Helgøy. Experimental investigations of freeze-bonds between saline ice-blocks: Ice-properties and reproducibility. 2012.

Henning Helgøy. Laboratory work on freeze-bonds in ice rubble, part 1: Experimental set-up, ice-properties and freeze-bond texture. *Port and Ocean Engineering under Arctic Conditions*, 2013.

P. Liferov and B. Bonnemaire. Ice rubble behaviour and strength: Part i. review of testing and interpretation of results. *Cold Regions Science and Technology*, 41(2):135 – 151, 2005. ISSN 0165-232X. doi: http://dx.doi.org/10.1016/j.coldregions.2004.10.001. URL http://www.sciencedirect.com/science/article/pii/S0165232X04001107.

A Marchenko and C Chenot. Regelation of ice blocks in the water and on the air. In *Proceedings of the 20th International conference on Port and Ocean Engineering under Arctic Conditions (POAC)*, 2009.

Anders Møllegaard. Experimental study on freeze-bonds in laboratory made saline ice. 2012.

Ada HV Repetto-Llamazares, Knut V Høyland, and Karl-Ulrich Evers. Experimental studies on shear failure of freeze-bonds in saline ice: Part i. set-up, failure mode and freeze-bond strength. *Cold Regions Science and Technology*, 65(3):286–297, 2011a.

Ada HV Repetto-Llamazares, Knut V Høyland, and Ekaterina Kim. Experimental studies on shear failure of freeze-bonds in saline ice:: Part ii: Ice–ice friction after failure and failure energy. *Cold Regions Science and Technology*, 65(3):298–307, 2011b.

Erland M Schulson, Paul Duval, et al. *Creep and fracture of ice*. Cambridge University Press Cambridge, 2009.

Nicolas Serré. Mechanical properties of model ice ridge keels. *Cold Regions Science and Technology*, 67(3):89–106, 2011.

Svetlana Shafrova and Knut V Høyland. The freeze-bond strength in first-year ice ridges. small-scale field and laboratory experiments. *Cold Regions Science and Technology*, 54(1):54–71, 2008.

Lucie Strub-Klein, Nicolas Serré, and Knut Vilhelm Høyland. Physical and mechanical investigations of sea ice ridges in late summer in the fram strait. 2010.

GW Timco and RP Burden. An analysis of the shapes of sea ice ridges. *Cold Regions Science and Technology*, 25(1):65–77, 1997.

Appendices

Appendix A

Test results

Table A.1: Samples FT- fresh tri-axial

Series	T_{ice}	Δt	T_w	S_w	S_i	$T_{ice,FB}$	$T_{ice,end}$	Failure	σ_r	Max piston load	H	D
FT-1	-2.5	0.5	0.0	0.48	0.05	-0,9	X	FB	0,0069 - 0,0075	0,46	149	69
FT-2	-2.5	1	0.0	0.48	0.11	-0,9	X	FB	0,0070 - 0,0075	1,02	149	70
FT-3	-2.5	0.5	0.0	0.44	0.04	-2,1	X	FB/ice	0,0200 - 0,0212	5,6	148,5	70
FT-4	-2.5	1	0.0	0.44	0.15	-1,4	X	FB	0,0202 - 0,0208	1,3	147,5	69
FT-5	-2.5	0.5	0.0	0.44	0.07	-2,2	X	FB/ice	0,0990 - 0,0998	4,78	148,2	70
FT-6	-2.5	1	0.0	0.44	0.01	-1,6	X	FB	0,0990 - 0,0994	2,85	148,2	71
FT-9	-8.5	5	-0.1	0.32	0.04	-5,4	X	FB	0,0070 - 0,0089	0,31	147,2	69
FT-10	-8.5	20	-0.1	0.32	0.03	-6,5	X	FB	0,0069 - 0,0094	1,04	147,8	71
FT-11	-8.5	60	-0.1	0.32	0.03	-5,8	X	FB	0,0071 - 0,0090	0,75	148	70
FT-12	-8.5	1200	-0.1	0.32	0.02	-5,0	X	FB	0,0071 - 0,0079	1.88	148	69
FT-13	-8.5	0.5	-0.1	0.38	0.03	-5,2	X	ice	0,0350 - 0,0404	5,44	148	66
FT-14	-8.5	1	-0.1	0.38	0.03	-4,6	X	FB	0,0347 - 0,0496	3,25	147,9	70,5
FT-15	-8.5	5	-0.1	0.35	0.03	-2,9	X	FB	0,0200 - 0,0209	1,45	147,3	68
FT-16	-8.5	20	-0.1	0.35	0.03	-3,8	X	FB	0,0200 - 0,0209	0,92	147,3	70
FT-17	-8.5	60	-0.1	0.35	0.02	X	X	FB	0,0200 - 0,0209	0,56	147,3	70
FT-18	-8.5	1200	0.0	0.32	0.03	-0,8	X	FB	0,0200 - 0,0205	0,97	147,5	68,5
FT-19	-8.5	0.5	-0.1	0.38	0.04	-4,4	X	FB	0,0573 - 0,0690	3,27	148	70
FT-20	-8.5	1	-0.1	0.38	0.06	-4,1	X	FB	0.1010 - 0.1173	5,93	147,1	71
FT-21	-8.5	5	-0.1	0.35	0.03	-3,1	X	FB	0,0991 - 0.1019	3,82	147,5	68,5
FT-22	-8.5	20	-0.1	0.35	0.02	-0,5	X	FB	0.0988 - 0.1026	2,14	147,1	70
FT-23	-8.5	60	-0.1	0.35	0.03	-0,7	X	FB	0,0987 - 0.1023	2,5	148	67,5
FT-24	-8.5	1200	-0.1	0.35	X	-1,4	X	FB	0.0994 - 0.1002	2,39	147	70

Table A.2: Samples ST- saline tri-axial

| Series	T_{ice}	Δt	T_w	S_w	S_i	$T_{ice,FB}$	$T_{ice,end}$	Failure	σ_r	Max piston load	H	D
ST-1a	-2.5	0.5	-0.5	7.85	2.31	-3.0	X	FB	0,0070 - 0,0094	5,4	149,5	71
ST-1b	-2.5	0.5	-0.4	7.85	1.70	-2.8	X	FB	0,0070 - 0,0078	0,37	149,5	72
ST-2a	-2.5	1	-0.5	7.85	2.12	-2.7	X	FB	0,0070 - 0,0078	5.0	149	71,5
ST-2b	-2.5	1	-0.4	7.85	1.63	-2.9	X	FB/ice	0,0070 - 0,0084	1,95	149,5	72
ST-3	-2.5	5	-0.5	7.85	2.58	-2.1	X	FB	0,0071 - 0,0076	3,44	149,2	71
ST-4	-2.5	20	-0.5	7.85	2.25	-1.2	X	FB	0,0069 - 0,0078	1,25	149,2	71
ST-5	-2.5	60	-0.5	7.85	2.24	-1,1	X	FB	0,0070 - 0,0078	0,77	149,2	71
ST-6a	-2.5	1200	-0.5	8,55	X	-0,5	-0,6	FB	0,0070 - 0,0076	0,69	149	71
ST-6b	-2.5	1200	-0.5	8,62	1.56	X	X	FB	X	X	149	71,5
ST-7	-2.5	0.5	-0.5	8,73	2.30	-2,6	-2,9	FB	0,0201 - 0,0205	3,2	149,5	71
ST-8	-2.5	1	-0.5	8,73	2.80	-2,9	-2,6	FB	0,0200 - 0,0207	7.0	149,5	71,5
ST-9	-2.5	5	-0.5	8,73	2.21	-2,3	-1,6	FB	0,0200 - 0,0207	2,8	149,5	71
ST-10	-2.5	20	-0.5	8,69	2.59	-1,4	-1,4	FB	0,0200 - 0,0208	0,83	149,5	71
ST-11	-2.5	60	-0.5	8,83	1.32	-1.1	-0,9	FB	0,0200 - 0,0209	2,7	149,2	71
ST-12	-2.5	1200	-0.5	8,55	1.20	-0,5	-0,5	FB	0,0200 - 0,0205	1,24	149,2	71
ST-13	-2.5	0.5	-0.5	8,24	1.60	-2,3	-2,3	FB	0,0988 - 0.1005	2,0	149,5	71
ST-14	-2.5	1	-0.5	8,24	2.50	-2,4	-2,5	FB	0,0990 - 0.1002	3,9	149,5	71
ST-15	-2.5	5	-0.5	8,24	0.72	-2,1	-1,8	FB	0,0991 - 0.1005	2.0	149,5	71,5
ST-16	-2.5	20	-0.4	8,66	1.08	-1.0	-1,3	FB	0,0990 - 0.1002	2,3	149,5	71
ST-17a	-2.5	60	X	X	X	X	X	X	X	X	148,2	71
ST-17b	-2.5	60	-0.5	8,24	2.61	-1,1	-0,9	FB	0,0990 - 0,0994	X	149,5	71,5
ST-18a	-2.5	1200	X	X	X	X	X	X	X	X	148,2	71
ST-18b	-2.5	1200	-0.5	8,85	0.97	-0,6	-0,6	FB	no pressure	X	149,2	71,5
ST-19	-8.5	0.5	-0.5	7.50	2.53	-5,8	-5,8	FB	0,0070 - 0,0078	2,42	148,5	72
ST-20	-8.5	1	-0.5	7.50	2.59	-4,8	-4,6	FB	0,0071 - 0,0078	3,78	149	71,5
ST-21	-8.5	5	-0.5	7.50	1.93	X	X	FB	0,0071 - 0,0085	11,25	149,5	72
ST-22	-8.5	20	-0.5	7.50	2.33	-2,4	-1,6	FB	0,0071 - 0,0076	4,76	149,5	71
ST-23	-8.5	60	-0.5	7.50	2.07	-1,3	-1,1	FB	0,0069 - 0,0078	3,43	149,8	71
ST-24	-8.5	1200	-0.5	7.50	1.69	-0,7	-0,9	FB	0,0070 - 0,0076	1,16	149	71
ST-25	-8.5	0.5	-0.5	8.50	2.72	-4,6	-3,6	FB	0,0199 - 0,0204	5,27	149,1	71,5
ST-26	-8.5	1	-0.5	8.50	2.76	-3,4	-4,3	FB	0,0200 - 0,0204	8,34	150	71,5
ST-27	-8.5	5	-0.5	8.50	0.56	-2,6	-3,1	FB	0,0199 - 0,0205	7,48	149,9	71,5
ST-28	-8.5	20	-0.5	8.50	2.70	-2.0	-1,7	FB	0,0200 - 0,0204	0.94	149,5	71
ST-29	-8.5	60	-0.5	8.50	0.75	-1,3	-1,3	FB	0,0201 - 0,0205	0.65	149,8	70,5
ST-30	-8.5	1200	-0.5	7.50	X	X	X	FB	0,0201 - 0,0205	1,85	150	71
ST-31	-8.5	0.5	-0.6	8.50	2.64	-4,7	-5,3	FB	0,0988 - 0,0990	11.3	149	71,5
ST-32	-8.5	1	-0.6	8.50	2.96	-3,7	-3,7	FB	0,0987 - 0,0992	8.4	149,5	70,5
ST-33	-8.5	5	-0.6	8.50	2.86	-2,6	-3,3	FB	0,0987 - 0,0992	8.4	149	72
ST-34	-8.5	20	-0.5	7.24	X	-1,9	-2,3	FB	0.993 - 1.000	5.25	150	71
ST-35	-8.5	60	-0.5	7.24	X	-1.3	-1.3	FB	0.993 - 0.998	2.74	150	71
ST-36	-8.5	1200	-0.6	8.50	2.31	-0.8	-0.8	FB	0,0988 - 0,0994	2.66	148,9	70,5

Table A.3: Samples Uni-axial, FU- fresh uni-axial, SU- saline uni-axial

Series	T_{ice}	Δt	T_w	S_w	S_i	$T_{ice,FB}$	$T_{ice,end}$	Failure	σ_r	Max piston load	H	D
FU-1	-8.5	0.5	-0.1	0.37	0.04	-4.9	X	FB/ice	0	2.26	175	70.5
FU-2	-8.5	1	-0.1	0.37	0.03	-4.7	X	FB	0	1.92	174	70
FU-3	-8.5	0.5	-0.1	0.37	0.03	-4.6	X	Ice	0	2.89	147	70
FU-4	-8.5	1	-0.1	0.38	0.03	-3.8	X	FB/ice	0	5,43	148	66
FU-5	-8.5	5	-0.1	0.38	0.03	-0.8	X	FB	0	1.24	147	69
SU-1	-8.5	0.5	-0.5	8.44	0.04	-5.3	-6.1	ice	0	5.05	175	71
SU-1$_2$	-8.5	0.5	-0.5	8.58	0.04	-5.0	-6.4	ice	0	8.38	175	71
SU-2	-8.5	1	-0.5	8.58	0.04	-4.7	-4.3	ice	0	6.1	175	71
SU-3	-8.5	5	-0.5	8.65	0.04	-2.6	-2.6	FB	0	4.8	175	71
SU-4	-8.5	20	-0.5	8.61	0.04	-2.1	-2.3	FB	0	4.8	175	71
SU-5	-8.5	0.5	-0.5	8.63	0.04	-5.6	-5.1	FB	0	6.6	150	71
SU-6	-8.5	1	-0.5	8.63	0.04	-4.9	-5.4	ice	0	6.0	150	71.5
SU-7	-8.5	5	-0.5	8.72	0.04	-3.0	-2.7	FB	0	4.6	150	71
SU-8	-8.5	20	-0.6	8.50	0.04	-0.8	-0.8	FB	0	1.3	148,9	70,5

B1

Appendix B

Figures of failure slopes for peak stresses
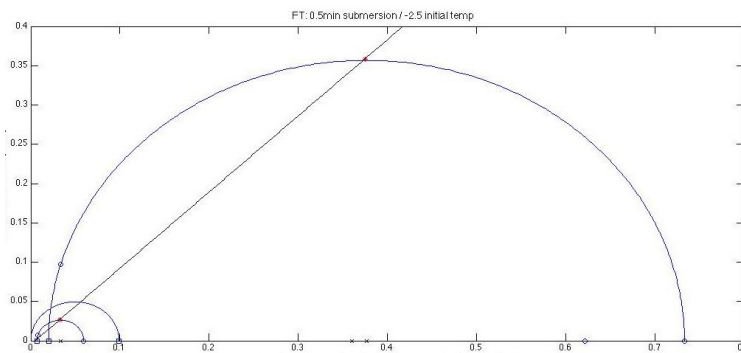
(a) Fresh config: T_i=-2.5°C and Δt=0.5min. Highest confinement reduced to uni-axial sample
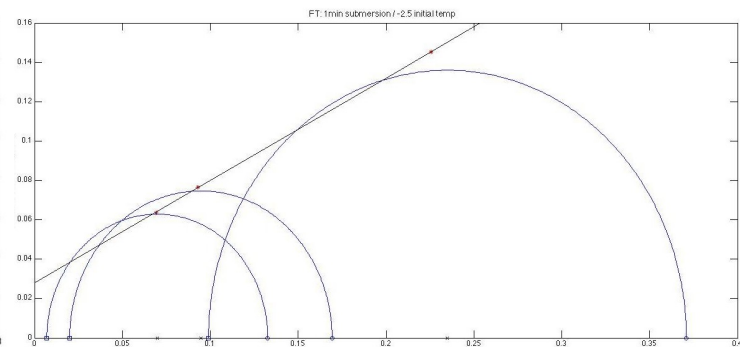
(b) Fresh config: T_i=-2.5°C and Δt=1min
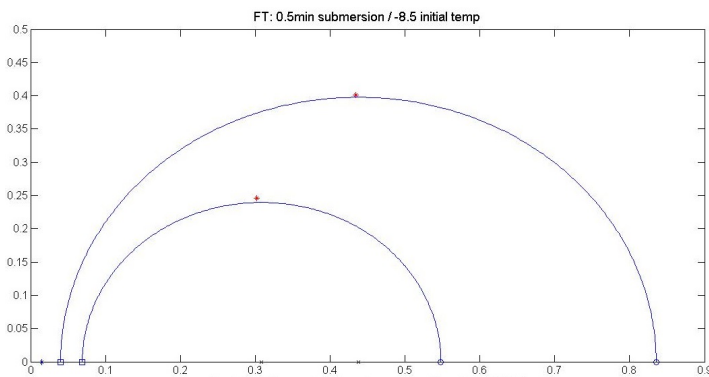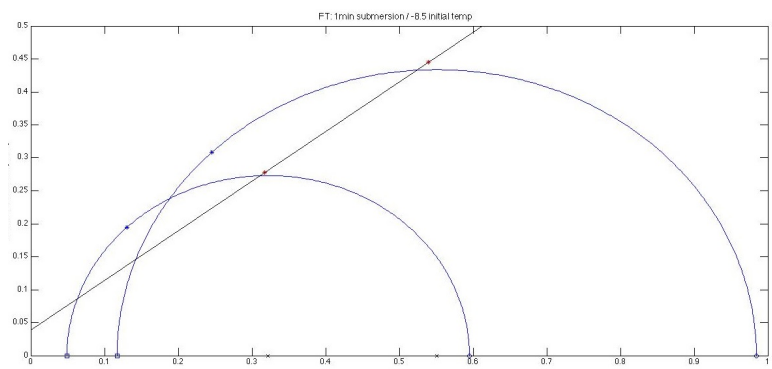
(c) Fresh config: T_i=-8.5°C and Δt=0.5min

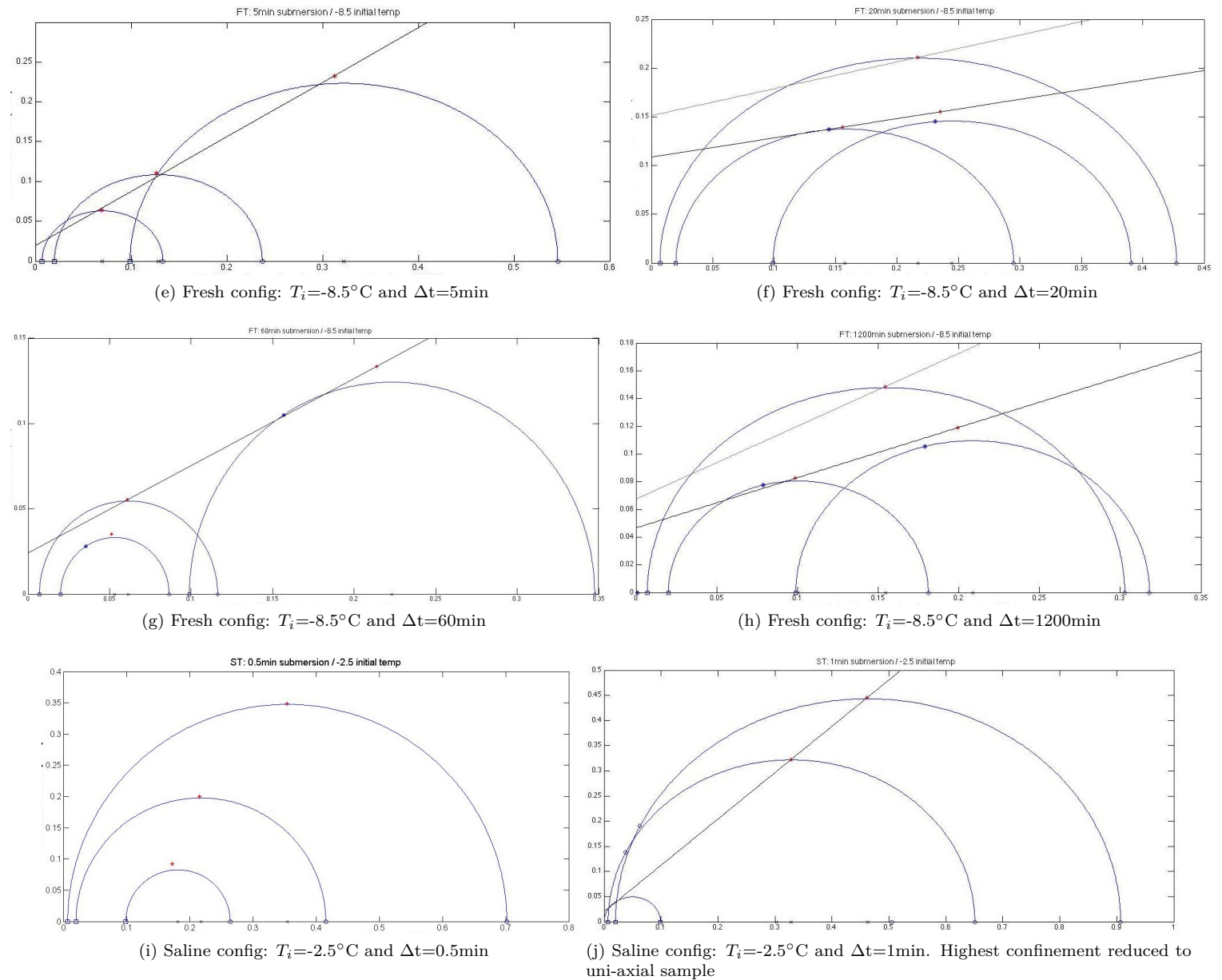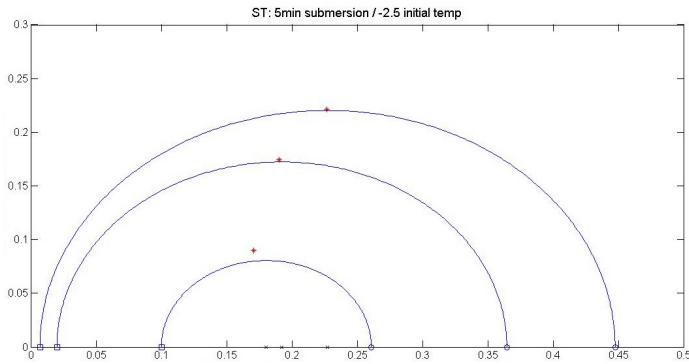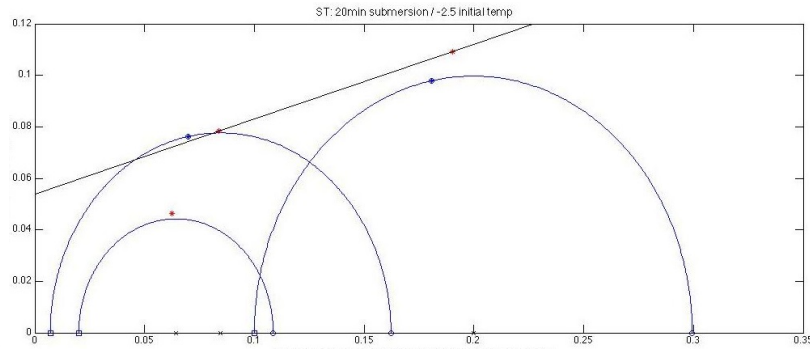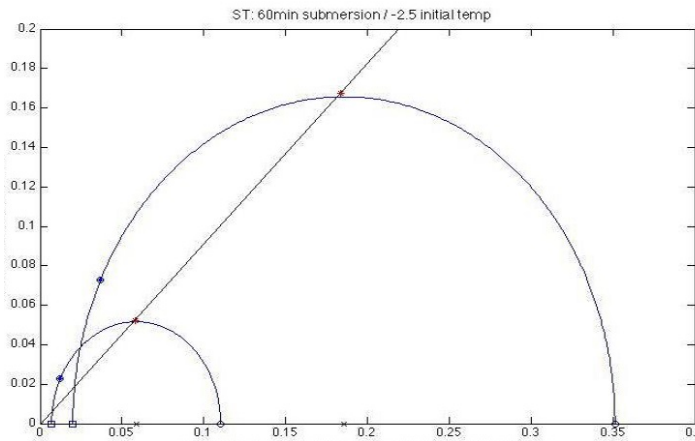(d) Fresh config: T_i=-8.5°C and Δt=1min

Figure B.1: Failure slopes of all configurations for peak stresses [MPa]. Blue mohr-circle indicates the uni-axial tests. Black line indicates the failure slope and the grey line indicates the failure slope of softening.
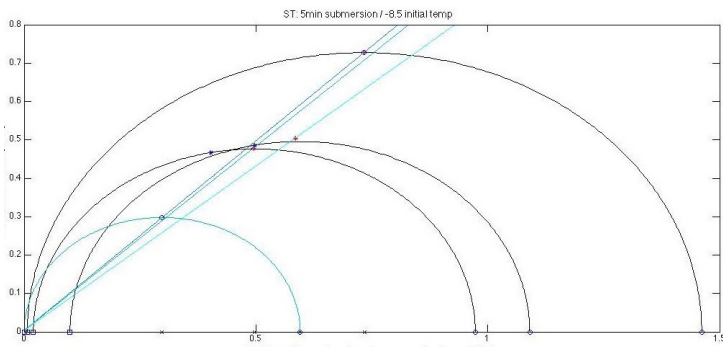
(e) Fresh config: T_i=-8.5°C and Δt=5min

(f) Fresh config: T_i=-8.5°C and Δt=20min

(g) Fresh config: T_i=-8.5°C and Δt=60min

(h) Fresh config: T_i=-8.5°C and Δt=1200min

(i) Saline config: T_i=-2.5°C and Δt=0.5min

(j) Saline config: T_i=-2.5°C and Δt=1min. Highest confinement reduced to uni-axial sample

Figure B.1: Failure slopes of all configurations for peak stresses [MPa]. Blue mohr-circle indicates the uni-axial tests. Black line indicates the failure slope and the grey line indicates the failure slope of softening.
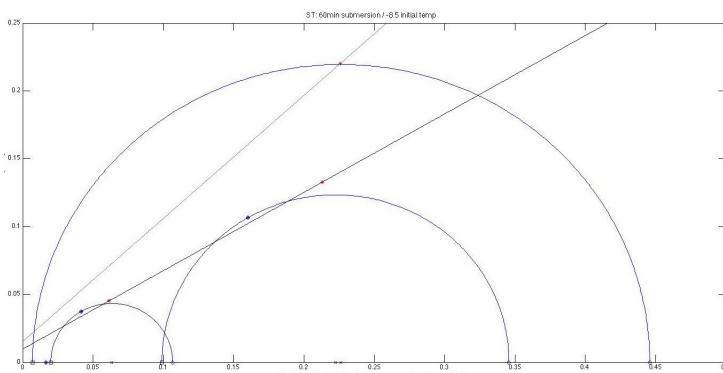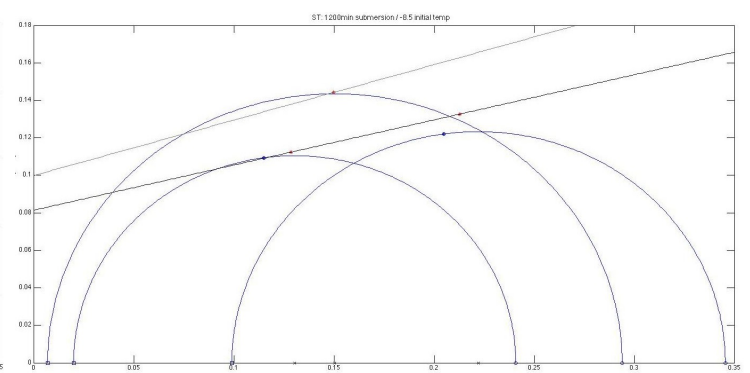
(k) Saline config: T_i=-2.5°C and Δt=5min

(l) Saline config: T_i=-2.5°C and Δt=20min

(m) Saline config: T_i=-2.5°C and Δt=60min
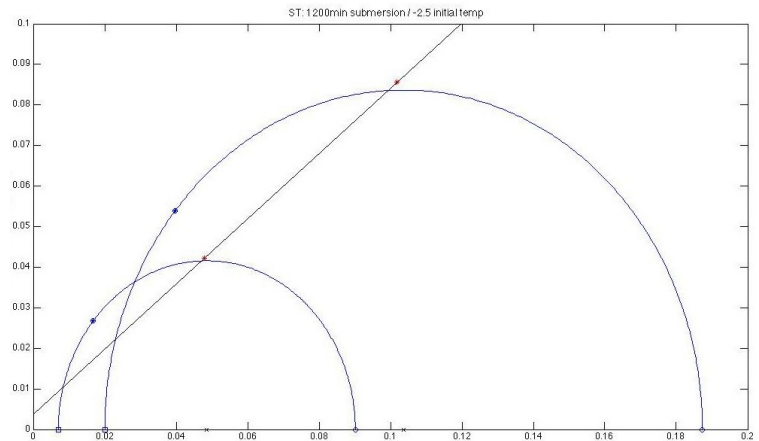
(n) Saline config: T_i=-2.5°C and Δt=1200min
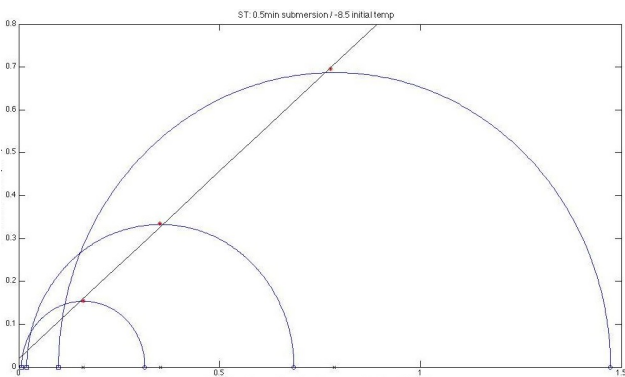
(o) Saline config: T_i=-8.5°C and Δt=0.5min
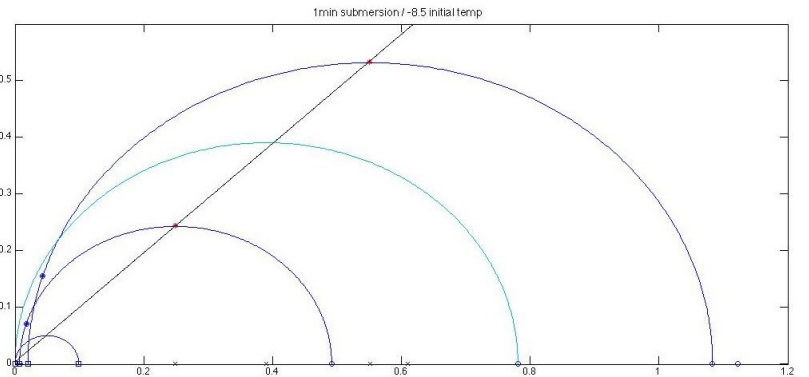
(p) Saline config: T_i=-8.5°C and Δt=1min. Highest confinement reduced to uni-axial sample

Figure B.1: Failure slopes of all configurations for peak stresses [MPa]. Blue mohr-circle indicates the uni-axial tests. Black line indicates the failure slope and the grey line indicates the failure slope of softening.

(q) Saline config: T_i=-8.5°C and Δt=5min
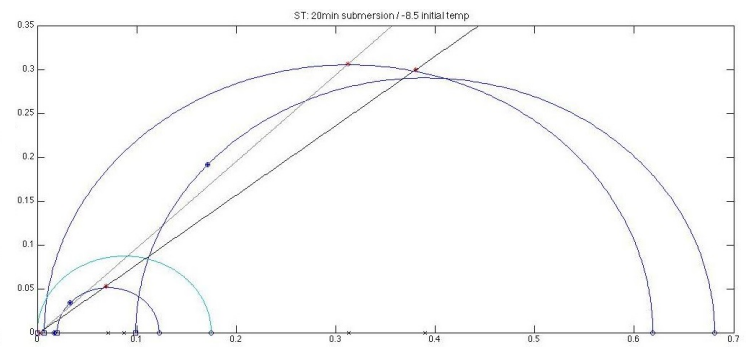
(r) Saline config: T_i=-8.5°C and Δt=20min

(s) Saline config: T_i=-8.5°C and Δt=60min

(t) Saline config: T_i=-8.5°C and Δt=1200min

Figure B.1: Failure slopes of all configurations for peak stresses [MPa]. Blue mohr-circle indicates the uni-axial tests. Black line indicates the failure slope and the grey line indicates the failure slope of softening.

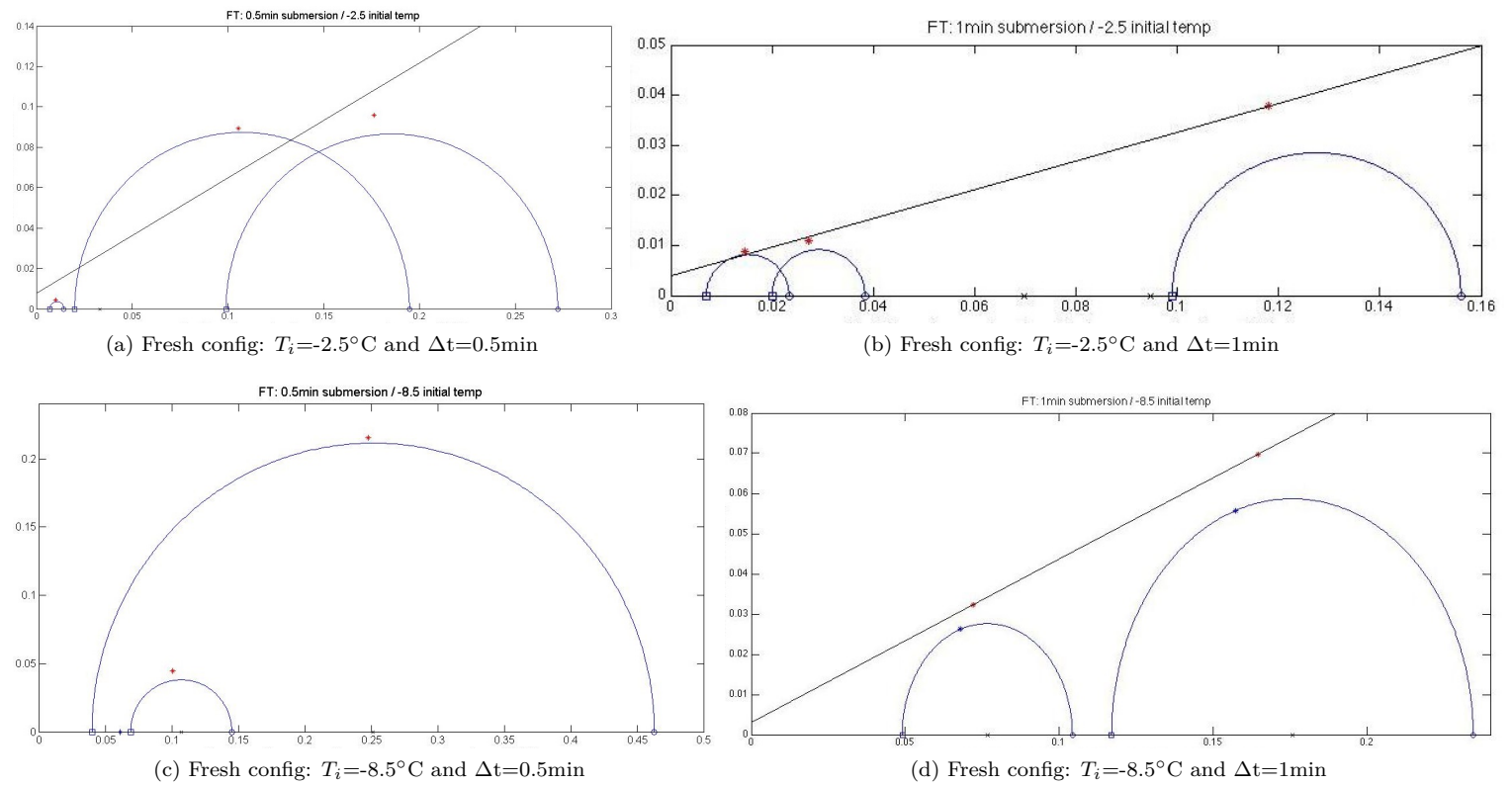# Appendix C

Figures of failure slopes for residual stresses

(a) Fresh config: T_i=-2.5°C and Δt=0.5min

(b) Fresh config: T_i=-2.5°C and Δt=1min

(c) Fresh config: T_i=-8.5°C and Δt=0.5min

(d) Fresh config: T_i=-8.5°C and Δt=1min

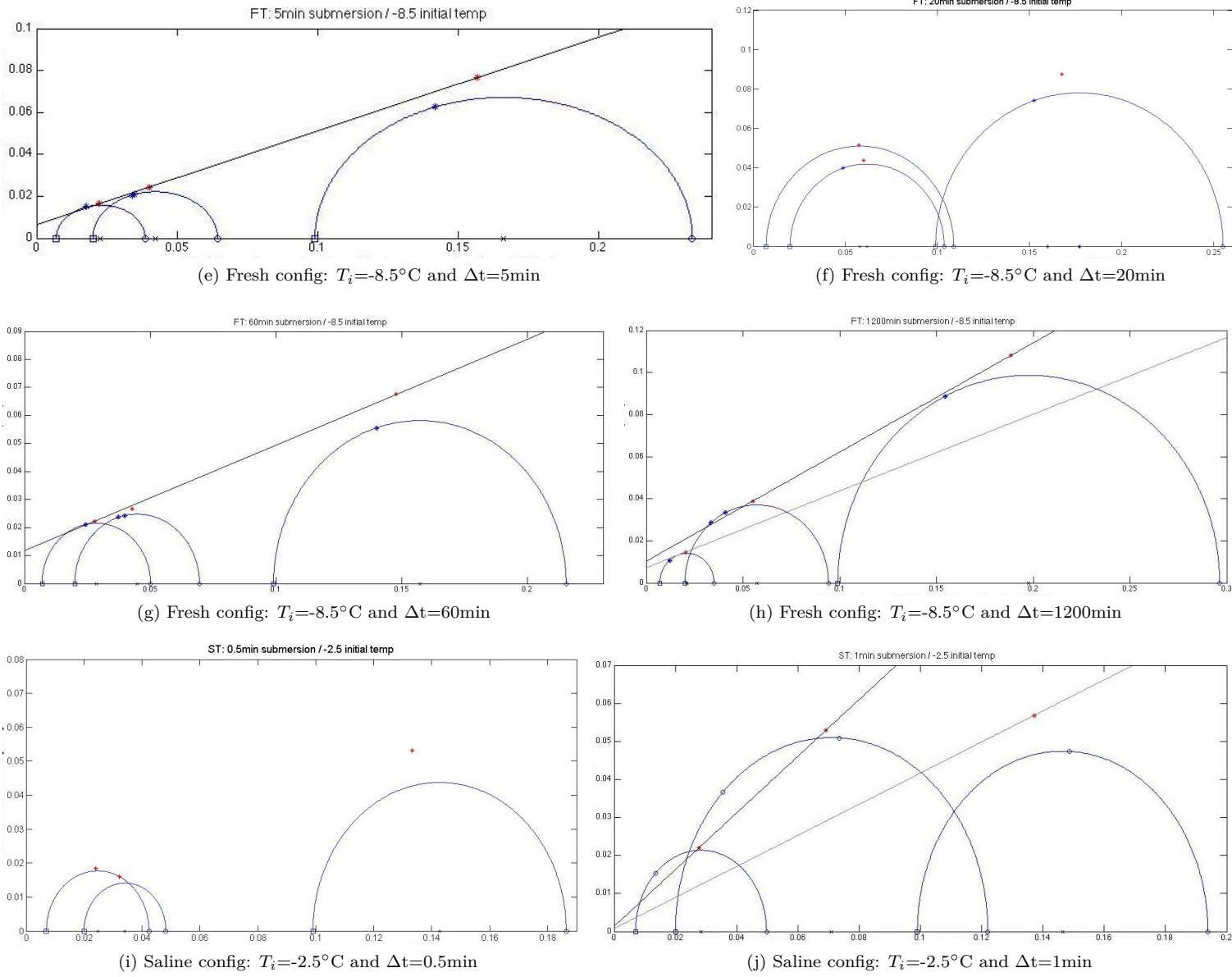Figure C.1: Failure slopes of all configurations for residual stresses [MPa]
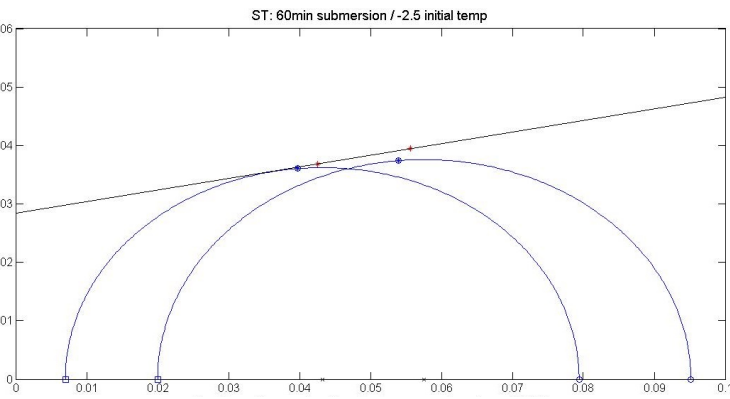
(e) Fresh config: T_i=-8.5°C and Δt=5min

(f) Fresh config: T_i=-8.5°C and Δt=20min

(g) Fresh config: T_i=-8.5°C and Δt=60min

(h) Fresh config: T_i=-8.5°C and Δt=1200min

(i) Saline config: T_i=-2.5°C and Δt=0.5min

(j) Saline config: T_i=-2.5°C and Δt=1min

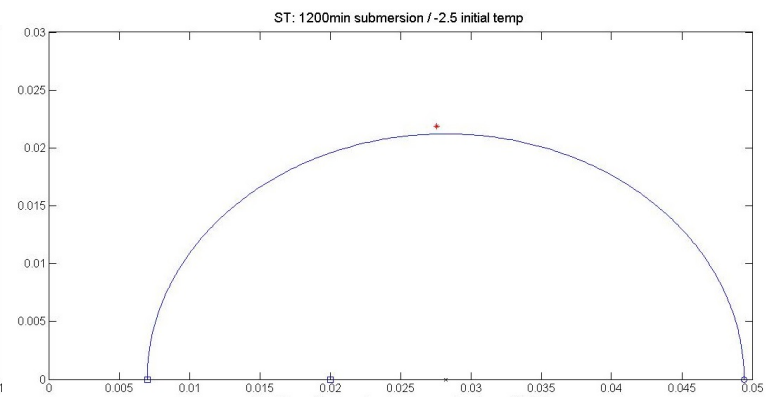Figure C.1: Failure slopes of all configurations for residual stresses [MPa]

(k) Saline config: T_i=-2.5°C and Δt=5min
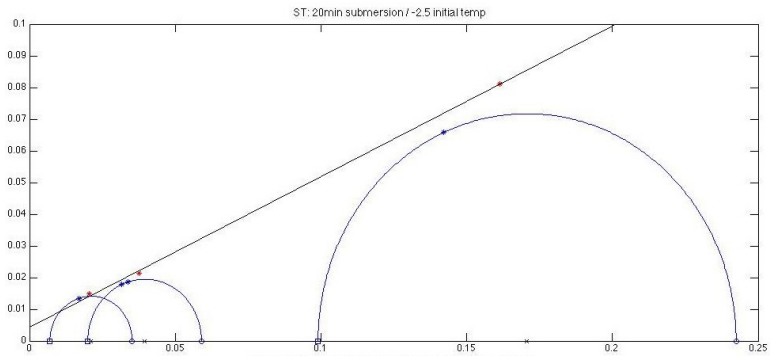
(l) Saline config: T_i=-2.5°C and Δt=20min

(m) Saline config: T_i=-2.5°C and Δt=60min

(n) Saline config: T_i=-2.5°C and Δt=1200min

(o) Saline config: T_i=-8.5°C and Δt=0.5min

(p) Saline config: T_i=-8.5°C and Δt=1min

Figure C.1: Failure slopes of all configurations for residual stresses [MPa]
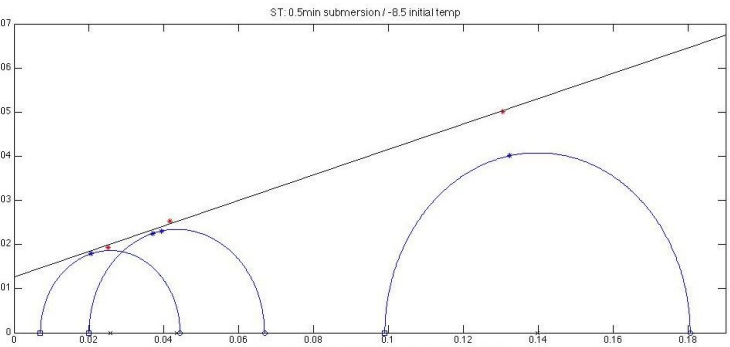
(q) Saline config: T_i=-8.5°C and Δt=5min
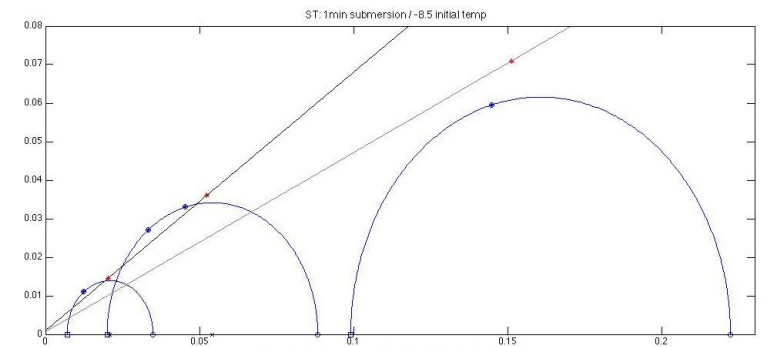
(r) Saline config: T_i=-8.5°C and Δt=20min

(s) Saline config: T_i=-8.5°C and Δt=60min
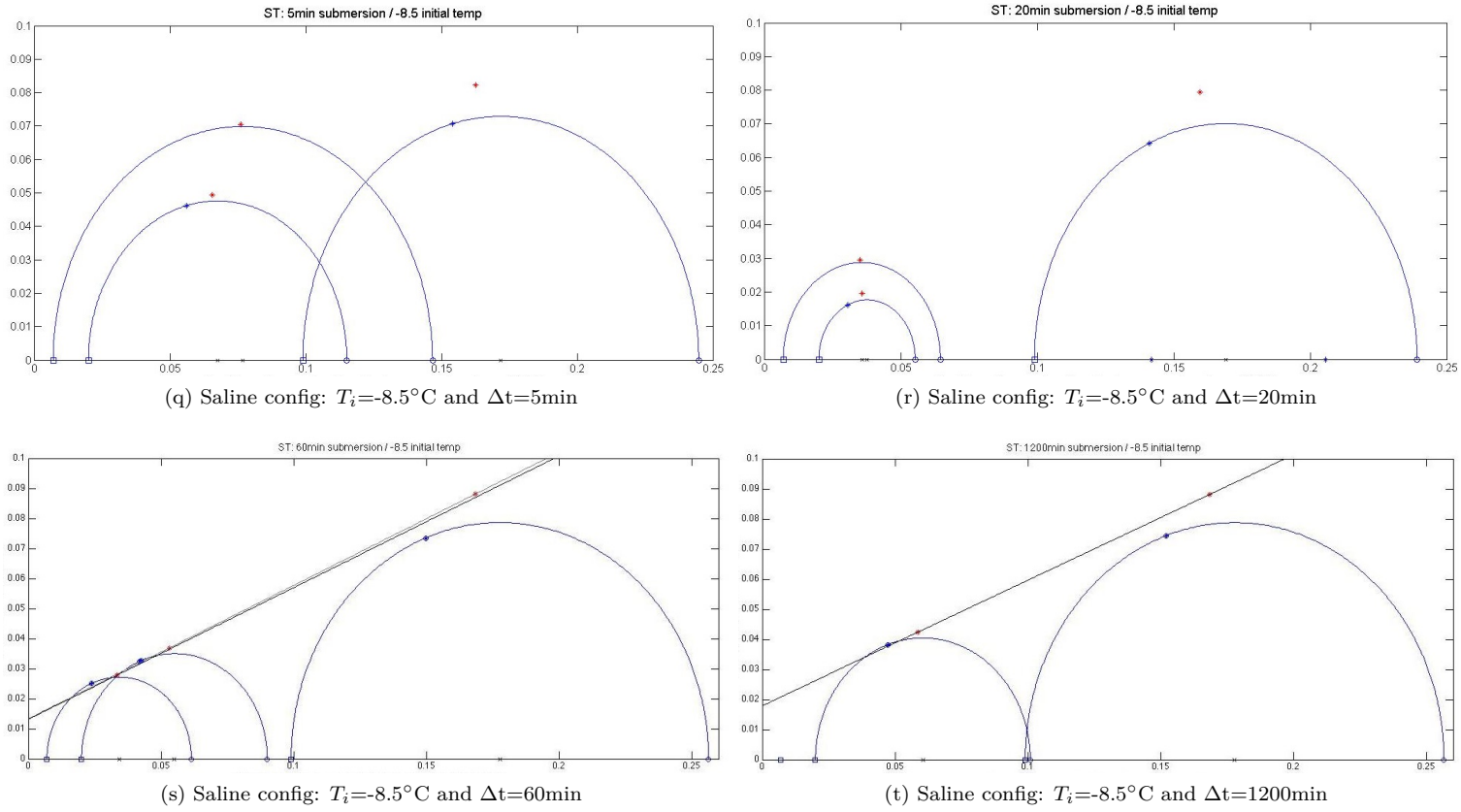
(t) Saline config: T_i=-8.5°C and Δt=1200min

Figure C.1: Failure slopes of all configurations for residual stresses [MPa]

Appendix D

Cohesion (c) and internal friction ϕ values for all configurations

Table D.1: Cohesion and friction angles for all peak stress configurations

	T_i	Δt	Type	c	ϕ
Fresh configurations	-2.5°C	0.5	2	-00047	44.10°
		1	1	0.0278	27.53°
	-8.5°C	0.5	2	-	-
		1	1	0.039	36.94°
		5	1	0.0195	34.94°
		20	4	0.1513	15.40°
		60	5	0.0241	27.13°
		1200	4	0.0675	27.72°
Saline configurations	-2.5°C	0.5	3	-	-
		1	2	0.0203	42.64°
		5	3	-	-
		20	5	0.0539	16.21°
		60	1	-0,00082	42.50°
		1200	1	0.0037	38.81°
	-8.5°C	0.5	1	0.02	41.16°
		1	2	0.003	43.98°
		5	4	0.4415	21.33°
		20	4	-0.0024	44.70°
		60	4	0.0153	42.21°
		1200	4	0.0999	16.47°

Table D.2: Cohesion and friction angles for all residual stress configurations

	T_i	Δt	Type	c	ϕ
Fresh configurations	-2.5°C	0.5	2	0.0077	29.70°
		1	1	0.0040	15.95°
	-8.5°C	0.5	2	-	-
		1	1	0.0031	22.04°
		5	1	0.0063	24.10°
		20		-	-
		60	1	0.0117	20.71°
		1200	4	0.0103	27.42°
Saline configurations	-2.5°C	0.5	3	-	-
		1	2	0.0014	36.70°
		5	3	0.0124	13.14°
		20	1	0.0043	25.41°
		60	1	0.0284	11.21°
		1200	1	-	-
	-8.5°C	0.5	1	0.0127	16.08°
		1	2	0.0010	33.85°
		5		-	-
		20		-	-
		60	1	0.0132	23.66°
		1200	1	0.0179	22.65°

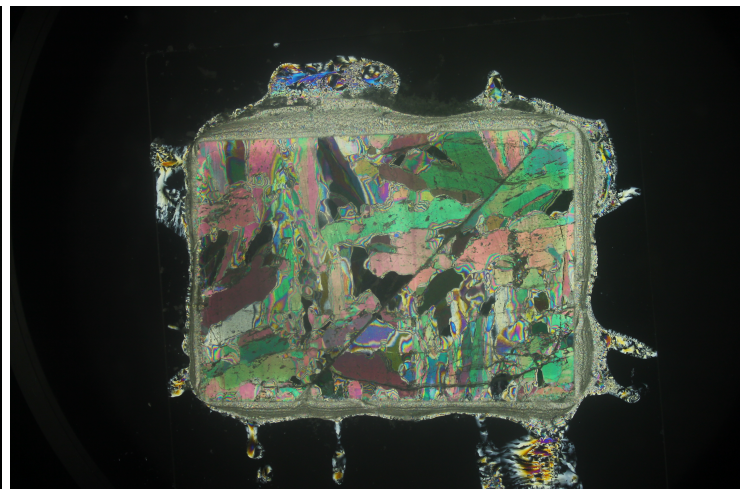E1

Appendix E

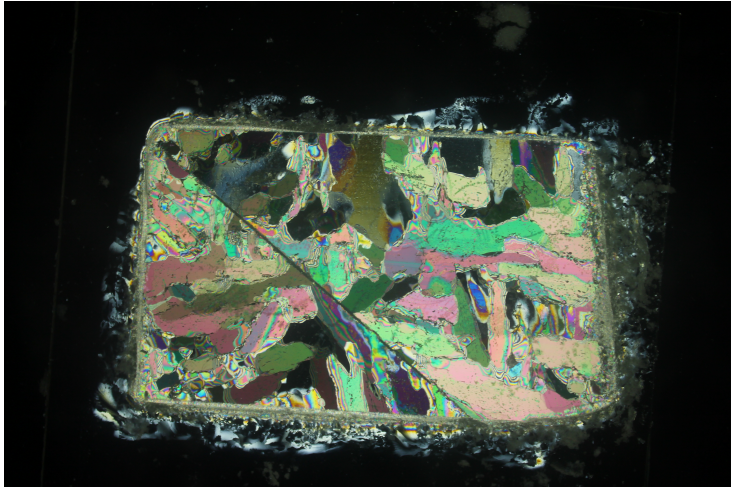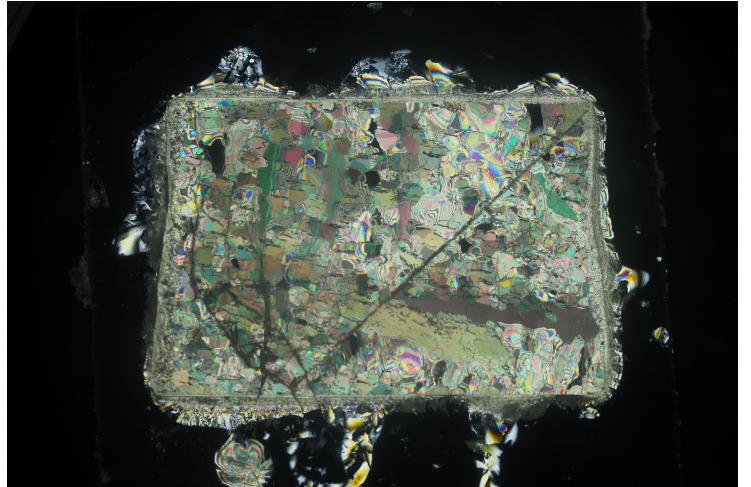# Freeze-bond thin sections
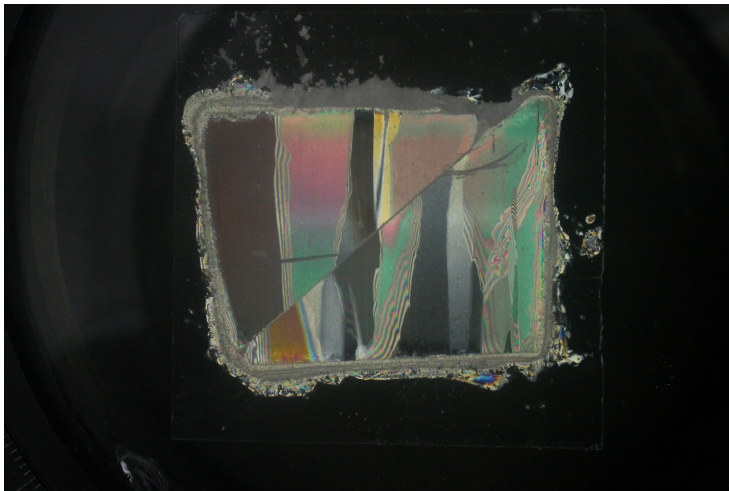
(a) FT-21
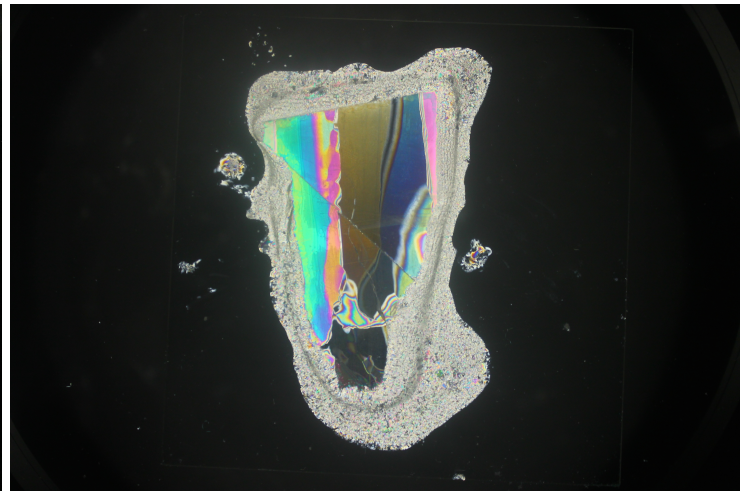
(b) FT-22
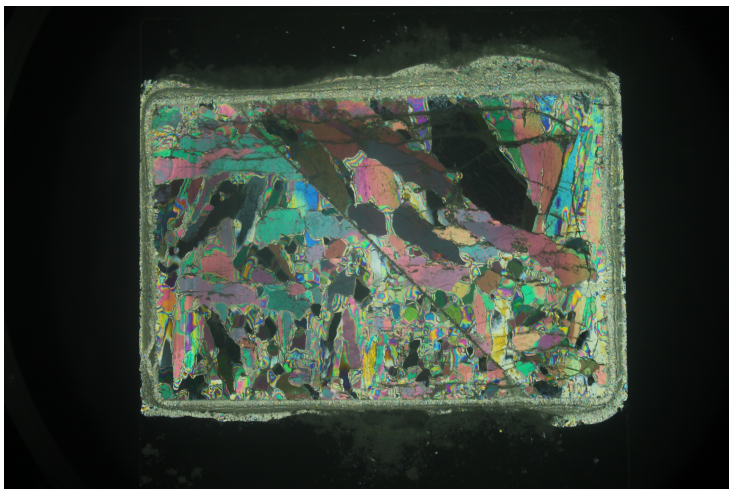
(c) ST-1

(d) ST-2

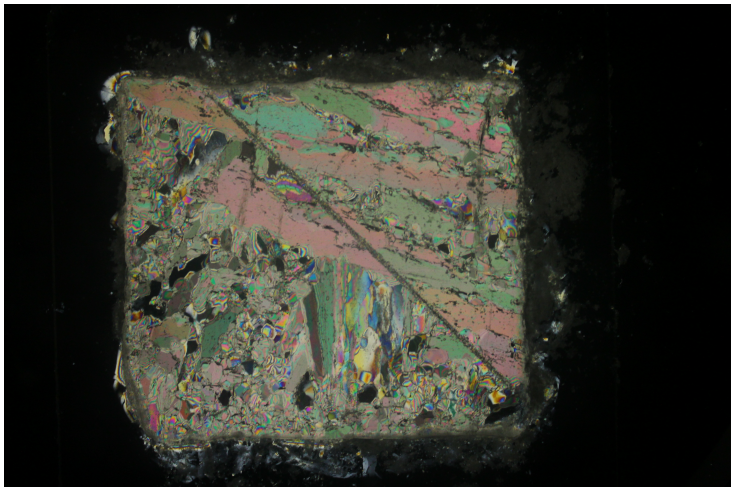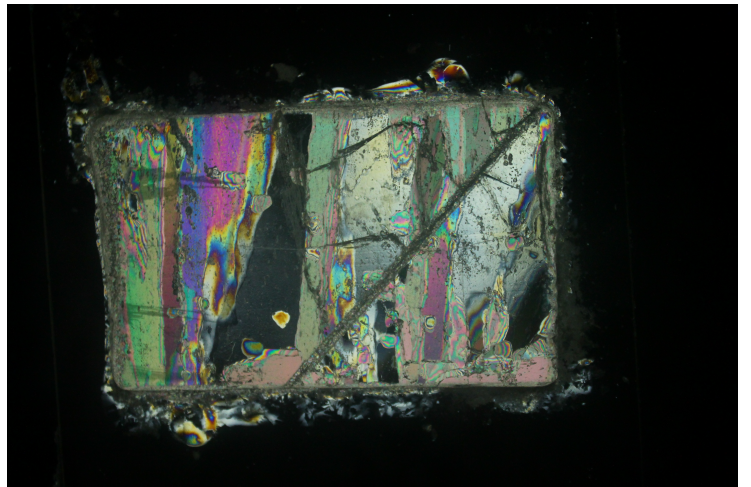Figure E.1: Thin section of freeze-bonds, samples after testing

(e) ST-4

(f) ST-10

(g) ST-16

(h) ST-28

Figure E.1: Thin section of freeze-bonds, samples after testing